Non-ionotropic signaling through the NMDA receptor GluN2B carboxy terminal domain drives morphological plasticity of dendritic spines and reverses fragile X phenotypes in mouse hippocampus

Running title: NMDA influence on spines, protein synthesis and fragile X

Stephanie A. Barnes[1,2], Aurore Thomazeau[1], Peter S.B. Finnie[1], Maxwell J Heinrich[1], Arnold J. Heynen[1], Noburu H. Komiyama[3,4,5], Seth G.N. Grant[3,4], Frank S. Menniti[6], Emily K. Osterweil[2,7], Mark F. Bear[1*]

Addresses:
[1]The Picower Institute for Learning and Memory, Massachusetts Institute of Technology, Cambridge, MA 02139, USA
[2] Centre for Discovery Brain Sciences, University of Edinburgh, Hugh Robson Building, George Square, Edinburgh EH8 9XD, UK
[3]Centre for Clinical Brain Sciences, University of Edinburgh, Edinburgh EH16 4SB, United Kingdom.
[4]Simons Initiative for the Developing Brain (SIDB), Centre for Discovery Brain Sciences, University of Edinburgh, Edinburgh. EH8 9XD. United Kingdom.
[5]The Patrick Wild Centre for Research into Autism, Fragile X Syndrome & Intellectual Disabilities, Centre for Discovery Brain Sciences, University of Edinburgh, Edinburgh EH8 9XD, United Kingdom.
[6]MindImmune Therapeutics, Inc., The George & Anne Ryan Institute for Neuroscience, University of Rhode Island, Kingston, RI 02881, USA
[7]F.M. Kirby Center for Neurobiology, Translational Neuroscience Center, Department of Neurology, Harvard Medical School, Boston Children's Hospital, Boston, MA 02115, USA

[*] To whom correspondence should be addressed: M.F.B. (Email: mbear@mit.edu)

46 pages, 7 figures, 1 supplemental figure
Abstract word count: 226
Introduction word count: 622
Discussion word count: 2496

Author contributions: SAB, AT, EKO and MFB designed research; SAB, AT, PSBF, AJH, and MJH performed research; SAB, AT, and MJH analyzed data; SAB and MFB wrote the paper; MFB and EKO supervised the project. The authors declare no conflict of interest.

Acknowledgements: Special thank you to Joseph Moskal for the helpful advice on Glyx-13. The authors are grateful to the FRAXA foundation and The Picower Institute Innovation Fund for supporting this research. Additional support was provided by NIH grant R21NS123499.

ABSTRACT

It is well known that activation of NMDA receptors (NMDAR) can trigger long-term synaptic depression (LTD) and that a morphological correlate of this functional plasticity is spine retraction and elimination. Recent studies have led to the surprising conclusion that NMDA-induced spine shrinkage proceeds independently of ion flux and requires the initiation of *de novo* protein synthesis, highlighting an unappreciated contribution of mRNA translation to non-ionotropic NMDAR signaling. Here we used NMDA-induced spine shrinkage in slices of mouse hippocampus as a readout to investigate this novel modality of synaptic transmission. By using subtype selective pharmacological and genetic tools, we find that structural plasticity is dependent on the ligand binding domain (LBD) of GluN2B-containing NMDARs and that metabotropic signaling occurs via the GluN2B carboxy terminal domain (CTD). Disruption of signaling by replacing the GluN2B CTD with the GluN2A CTD leads to an increase in spine density, dysregulated basal protein synthesis, exaggerated mGluR-LTD, and epileptiform activity reminiscent of phenotypes observed in the *Fmr1* knockout (KO) model of fragile X syndrome. By crossing the *Fmr1* KO mice with animals in which the GluN2A CTD has been replaced with the GluN2B CTD, we observe a correction of these core fragile X phenotypes. These findings suggest that non-ionotropic NMDAR signaling through GluN2B may represent a novel therapeutic target for the treatment of fragile X and related causes of intellectual disability and autism.

INTRODUCTION

N-methyl-d-aspartate receptors (NMDARs) play a crucial role in refining neural circuits that are established during development and modified during experience-dependent learning. These excitatory glutamatergic receptors mediate dynamic changes in synaptic connectivity, which include the controlled regulation of dendritic spine formation and enlargement, as well as spine retraction and elimination. Bidirectional changes in dendritic spine structure coincide with changes in synaptic strength. Enlargement of dendritic spines accompanies long-term potentiation (LTP), whereas spine shrinkage is observed after long-term depression (LTD). Considerable evidence suggests that perturbations in the maturation and plasticity of neuronal connections underlie neurological disorders associated with cognitive impairments. In agreement, numerous mutations in NMDAR subunits have been identified in patients with intellectual disability (ID), autism spectrum disorder (ASD), and epilepsy[1-3]. These findings indicate that NMDAR dysfunction may play a prominent role in the pathophysiology of neurodevelopmental disorders.

In the CA1 region of the hippocampus, NMDAR-dependent LTD and spine shrinkage can be induced by brief application of the agonist NMDA[4-6], low-frequency stimulation of identified input pathways[7-9], or by uncaging glutamate at single spines[10]. From these studies it has emerged that NMDARs can trigger intracellular events independently of ion permeation[11-13]. Although there are conflicting data on the requirement for Ca^{2+} flux to trigger NMDAR-LTD[10,14-23], numerous groups have consistently shown that structural plasticity is solely dependent on agonist binding, and occurs even in the presence of co-agonist and ion channel blockers[10,24]. Recent studies from this laboratory, in which the functional and structural effects of brief exposure to the receptor agonist NMDA were monitored simultaneously, confirmed that LTD and spine shrinkage mechanistically diverge[24]. NMDAR-LTD was abolished in the presence of the ion channel blocker MK-801, and by 7-CK an antagonist at the co-agonist binding site, while spine shrinkage remained intact. Together these findings indicate that the NMDAR can signal in both an ionotropic and non-ionotropic mode to trigger LTD and spine shrinkage, respectively. Non-ionotropic NMDAR signaling was originally described as "metabotropic"[14,25], so we have used the term "mNMDAR" to refer to this type of signaling[24].

Further examination of mNMDAR signaling revealed that spine shrinkage was dependent on the activation of mTORC1 and the synthesis of new proteins[24]. Dysregulated synaptic protein synthesis and altered spine structure are features of fragile X syndrome (FXS), a neurodevelopmental disorder characterized by ID and ASD, and caused by loss of the fragile X messenger ribonucleoprotein (FMRP)[26-28]. This structural readout of mNMDAR function was therefore investigated in the *Fmr1* KO mouse model of fragile X. Although the magnitude of spine shrinkage in response to NMDA appeared intact, it proceeded in the presence of cycloheximide,

consistent with the conclusion that the local protein synthesis that normally gates spine plasticity is dysregulated in this disorder[24].

There is much left to learn about mNMDARs and how they might contribute to pathophysiology in fragile X. In this study we have used spine shrinkage in response to NMDA as an assay to dissect the GluN2 subtype and structural motifs that transduce agonist binding to the initiation of mNMDAR signaling. The data show that ligand binding to the GluN2B subunit is obligatory, and that signaling is mediated via the GluN2B carboxy terminal domain (CTD). Eliminating mNMDAR signaling by replacing the GluN2B CTD with the GluN2A CTD phenocopies several core aspects of fragile X pathophysiology in the hippocampus; namely, increased density of dendritic spines, an elevated rate of bulk basal protein synthesis, exaggerated LTD mediated by G-protein coupled metabotropic glutamate receptors (mGluR-LTD) in area CA1, and increased epileptiform activity in area CA3. Conversely, augmenting mNMDAR signaling pharmacologically—or by crossing *Fmr1* KO mice with animals in which the GluN2A CTD is replaced with the GluN2B CTD—corrects protein synthesis, mGluR-LTD, and audiogenic seizure phenotypes. Together, the results suggest that GluN2B might be a novel therapeutic target in fragile X.

RESULTS

In hippocampal pyramidal neurons, NMDARs are tetramers consisting of two obligatory GluN1 and two GluN2 (A and B) subunits that co-assemble in to a di- or tri-heteromeric arrangement. Although GluN2B predominates at birth and is expressed throughout adulthood, GluN2A levels gradually increase during postnatal development and impose a distinct and dominant kinetic profile on the NMDAR assembly[29,30]. Since GluN2A/2B subunits have varied distributions and physiological roles, an important objective is to determine the subtype specificity of mNMDAR signaling and understand how it elicits structural plasticity at CA1 synapses. Study of the respective contribution of the GluN2 subtype is complex because deletion of *Grin2B* is lethal from birth and widespread loss leads to disruption in network activity[31,32]. Therefore, in addition to utilizing a constitutive *Grin2A* KO mouse line, we employed genetically engineered mice carrying conditional knockout alleles for GluN2A (*Grin2A*$^{fl/fl}$) and GluN2B (*Grin2B*$^{fl/fl}$) to determine the subtype specificity of mNMDAR signaling.

We simultaneously examined the contribution of the GluN2A subtype to NMDAR-dependent LTD and spine shrinkage in transverse hippocampal slices prepared from the progeny of *Grin2A* KO mice crossed with a Thy1-GFP line (P25-35). These mice express GFP in a random subset of neurons and using two-photon time-lapse fluorescence imaging we were able to visualize dendritic spines along isolated apical dendrites of CA1 pyramidal neurons in stratum radiatum. In addition, we performed extracellular recordings by stimulating the Schaffer collateral pathway every 30 seconds and recorded the corresponding field excitatory postsynaptic potentials (fEPSPs) from the region surrounding the dendrite of interest. To induce NMDAR-dependent LTD and spine shrinkage, we

briefly applied NMDA (20 μM, 3 min), which is known to trigger a saturating and persistent reduction in the fEPSP slope and spine volume[4,24].

GluN2B triggers non-ionotropic NMDAR signaling and the retraction of dendritic spines.
We observed that the acute application of NMDA induced a persistent depression of fEPSP responses in wild-type (WT) Thy1-GFP slices that was significantly reduced, but not fully abolished, in *Grin2A* KO Thy1-GFP mice (**Fig. 1A$_{i}$**). In contrast, NMDA triggered a reduction in spine volume that was indistinguishable between *Grin2A* KO and WT Thy1-GFP slices (**Fig. 1A$_{ii}$**). These findings suggest that GluN2A-containing assemblies play a role in functional NMDAR-LTD but are not required for the induction of spine shrinkage. Therefore, the GluN2B di-heteromers may be sufficient to initiate the non-ionotropic signaling that underlies NMDA-induced structural plasticity at CA1 synapses.

To test this hypothesis, juvenile *Grin2A* and *Grin2B* floxed mice (P25) received a transcranial injection into the dorsal hippocampus of an HSV expressing cre-eGFP fusion protein or HSV-eGFP control (**Fig. 1B**). After 5-7 days, hippocampal slices were prepared and imaged (**Fig. 1C**). Consistent with previous reports, we observed sparse eGFP signal throughout CA1 indicating that the HSV-Cre-eGFP eliminated the floxed *Grin2A or 2B* allele in a small population of pyramidal neurons in CA1[33]. In agreement with our findings from *Grin2A* KO Thy1-GFP mice, the acute application of NMDA led to a comparable reduction in spine volume in conditional *Grin2A$^{fl/fl}$* and control mice (**Fig. 1D**). However, conditional postnatal deletion of *Grin2B*, which spares only the GluN2A di-heteromeric receptors, abolished spine shrinkage at CA1 synapses (**Fig. 1E**). Thus, the GluN2B-containing receptors are obligatory and sufficient to induce mNMDAR signaling. Together, these findings indicate that GluN2A- and GluN2B-containing di- and tri-heteromeric assemblies contribute differentially to NMDAR-dependent functional and structural plasticity at CA1 synapses.

Pharmacology of NMDAR-mediated functional and structural plasticity indicates that agonist binding to GluN2B is critical for non-ionotropic signaling.
NMDAR subunits have a similar topology consisting of three transmembrane domains (TMD), one reenterant loop that comprises the channel pore, an extracellular amino-terminal domain (NTD), a ligand binding domain (LBD), and an intracellular carboxyl-terminal domain (CTD) that couples the receptor to intracellular signaling messengers[34]. The GluN2A and GluN2B subtypes show a high degree of similarity in their amino acid structures, particularly in their NTD and TMD (69%), making it difficult to pharmacologically isolate these subunits[35]. However, there are several compounds that show greater selectively towards GluN2A- or GluN2B-containing receptors (**Fig. 2A**).

Here, we utilized conantokin-G, a competitive antagonist of the GluN2B LBD, and MPX-004, a negative allosteric modulator (NAM) of GluN2A containing NMDARs[36,37]. We observed that blocking the GluN2B LBD with conantokin-G (2 μM), which leaves the LBD of GluN2A di-heteromers intact, eliminated 66% of the isolated NMDAR-mediated fEPSP (**Fig. 2B**) and abolished

both NMDA-induced LTD and spine shrinkage at CA1 synapses (**Fig. 2C$_{i-ii}$**). The LTD and spine findings are comparable to those using the non-selective, competitive antagonist D-APV[24]. These data suggest that activation of GluN2A di-heteromers alone is not sufficient to drive either NMDA-dependent functional or structural plasticity at CA1 synapses and supports the conclusion from the conditional genetic studies that GluN2B is essential for the mNMDAR signaling that culminates in spine shrinkage.

Next, we pharmacologically targeted GluN2A using the NAM MPX-004 (30 μM), which strongly inhibits ion flux through the GluN2A di- and tri-heteromeric assemblies[36,38]. We observed that MPX-004 caused a 47% block of the isolated NMDAR-fEPSP (**Fig. 2D**) and a comparable inhibition of LTD (**Fig. 2E$_{i}$**) but had no effect on spine shrinkage (**Fig. 2E$_{ii}$**). Together, the data suggest that GluN2A-containing receptors may substantially contribute to the induction of functional LTD, but spine shrinkage is solely dependent on agonist binding to the LBD of GluN2B-containing receptors.

Ro25-6981 binds to the NTD of GluN2B and allosterically limits ion flux through GluN2B diheteromeric receptors, with minimal effect on GluN2A/B triheteromeric receptors[39]. In our preparation, Ro25-6981 (30 μM) inhibited the NMDAR-mediated EPSC by 51%, but had no impact on the magnitude of either spine shrinkage or NMDA-induced LTD (**Supplemental Fig. 1)**. These findings are consistent with the conclusion that NMDA-induced spine shrinkage is triggered by activation of the LBD of GluN2B di- and tri-heteromeric receptors. Only when this LBD is blocked using the GluN2B selective competitive inhibitor conantokin-G do we see that spine shrinkage fully abolished.

NMDARs induce spine shrinkage through the GluN2B carboxyterminal domain.

As ligand binding alone can trigger mNMDAR signaling in the absence of ion flux, we hypothesized that it may be transduced through the CTD of GluN2B. While the NTD and TMD domains of GluN2A and GluN2B are highly conserved, their large intracellular CTDs exhibit considerable sequence heterogeneity (~29% similarity)[35]. It has been previously reported that the GluN2B CTD is crucial for coupling the NMDAR assembly to a large complex of proteins and has distinct effects on synaptic plasticity and behavior relative to the GluN2A CTD[40]. Thus, we speculated that the CTDs may also be the locus for the difference in the abilities of GluN2B and GluN2A NMDAR assemblies to elicit mNMDAR signaling and spine retraction. To test this idea, we utilized a transgenic knockin line, where the exon encoding the CTD of GluN2A is deleted and replaced with the GluN2B CTD (GluN2A^{2BCTD}, "A2B"; **Fig. 3A**) and vice versa (GluN2B^{2ACTD}, "B2A"; **Fig. 3D**). Importantly, the NTD, LBD and TMD are left intact in GluN2A^{2BCTD} and GluN2B^{2ACTD} mice and switching the CTD has been reported to have no functional effect on NMDAR EPSCs or NMDA/AMPAR ratios in the hippocampus[40]. Crossing the GluN2A^{2BCTD} and GluN2B^{2ACTD} mice with the Thy1-GFP line enabled us to then examine structural plasticity downstream of NMDAR activation. We observed that deleting

the CTD of GluN2A and replacing it with GluN2B had no impact on spine shrinkage at CA1 synapses (**Fig. 3B**). In contrast, eliminating the CTD of GluN2B and replacing it with GluN2A abolished spine shrinkage in GluN2B^{2ACTD} mice relative to WT littermates (**Fig. 3E**). These findings suggest that NMDA triggers mNMDAR signaling through the GluN2B CTD of di-heteromeric assemblies.

During development, a failure to refine neural circuitry in an activity-dependent manner has been shown to lead to an overabundance of dendritic spines that yields excessive excitatory synapses[41]. Therefore, we speculated whether there may be an abnormality in dendritic spine density in GluN2B^{2ACTD} mice due to the loss of NMDAR-induced spine shrinkage and elimination. To test this hypothesis, we quantified spine density along the apical dendrites of CA1 pyramidal neurons in GluN2A^{2BCTD} and GluN2B^{2ACTD} mice. We observed no significant difference in spine density between GluN2A^{2BCTD} and WT slices (**Fig. 3C**), but in the absence of the 2B CTD there was a subtle, but significant, increase in spine density in GluN2B^{2ACTD} mice relative to WT controls (**Fig. 3F**).

GluN2B CTD bidirectionally regulates protein synthesis and mGluR-LTD.

Previously, we have shown that spine shrinkage is sensitive to the mRNA translational inhibitor cycloheximide and the mTORC1 inhibitor rapamycin. These findings suggested that mNMDAR signaling may trigger *de novo* protein synthesis via the mTORC1 pathway to support the persistent reduction in spine volume[24]. To directly measure mRNA translation, we performed a metabolic labeling assay in acute hippocampal slices that mimics conditions used to record long-term changes in functional and structural plasticity. Hippocampal slices were recovered in oxygenated ACSF for 4 hrs to allow metabolic processes to recover. Transcription was then blocked with actinomycin D (25 μM) for 30 mins to isolate mRNA translation, before newly synthesized proteins were labelled with ^{35}S-methionine/cysteine protein labeling mix (**Fig. 4A**). To determine whether the activation of NMDARs can drive changes in bulk protein synthesis, we stimulated slices with NMDA (20 μM, 3 mins) or vehicle during protein labeling and then transferred slices to ACSF containing ^{35}S methionine/cysteine for a further 27 minutes. We observed that NMDA caused a significant reduction in ^{35}S incorporation (**Fig. 4B**), whereas incubating hippocampal slices with the competitive antagonist D-APV (50 μM), 30 mins prior and throughout protein labeling, led to a significant increase in mRNA translation (**Fig. 4C**). These data demonstrate that targeting the LBD of NMDARs can bidirectionally regulate global protein synthesis rates in the hippocampus.

Based on these findings, we wanted to determine whether NMDARs can alter mRNA translation in the absence of ion flux. Hippocampal slices were incubated in ACSF containing actinomycin D ± MK-801 and then labelled with ^{35}S methionine/cysteine ± MK-801. During metabolic labeling slices were briefly stimulated with NMDA or vehicle ± MK-801. We observed that NMDA causes a significant reduction in ^{35}S incorporation in the presence of MK-801 (**Fig. 4D**). These findings suggest that NMDARs can alter translational rates in the absence of ion permeation to support spine shrinkage at CA1 synapses. Although it may seem paradoxical that bulk protein

synthesis is decreased by stimulating the mTORC1 pathway through GluN2B, these findings are consistent with previous studies in the *Tsc2* heterozygous mouse[42] and reflect a change in the balance between pools of mRNA competing for access to ribosomes[43].

Encouraged by these findings, we next wanted to examine whether switching the GluN2A and GluN2B CTD could influence protein synthesis rates under basal conditions in the absence of exogenous stimulation. We observed that deleting the GluN2B CTD and replacing it with GluN2A (GluN2B^{2ACTD}/B2A mice) led to a significant increase in protein synthesis relative to WT slices (**Fig. 4E**). Conversely, eliminating the GluN2A CTD and replacing it with 2B (GluN2A^{2BCTD}/A2B mice), significantly reduced protein synthesis in GluN2A^{2BCTD} heterozygous and homozygous mice in a gene dose-dependent manner (**Fig. 4F**). Together these findings suggest that the GluN2 CTD regulates basal protein synthesis levels in the hippocampus.

One form of synaptic plasticity that is sensitive to alterations in protein synthesis is mGluR-LTD[44]. Increases in bulk protein synthesis, observed in mouse models of fragile X and *Syngap1* haploinsufficiency, coincide with an elevation in mGluR-LTD that is no longer gated by new protein synthesis[27,45,46]. In contrast, decreases in bulk protein synthesis, as observed in *Tsc2* heterozygous mice, lead to an impairment in mGluR-LTD[42]**.** Together they define an axis of synaptic pathophysiology, where deviations in protein synthesis can be used to predict disease related cellular abnormalities. Therefore, we hypothesized that protein synthesis-dependent phenotypes may be disrupted in GluN2B^{2ACTD} and GluN2A^{2BCTD} mice, mimicking *Fmr1* KO and *Tsc*2 heterozygous mice, respectively.

To test this hypothesis, we examined mGluR-LTD in GluN2B^{2ACTD} and GluN2A^{2BCTD} mice. Acute hippocampal slices were prepared and recovered for 3-4 hours before extracellular recordings were performed in CA1. Once a steady baseline was obtained, mGluR-LTD was induced by the acute application of the group 1 mGluR$_{1/5}$ agonist dihydroxyphenylglycine (DHPG; 50 μM, 5 mins[47]), and the slope of fEPSPs were monitored for a further 55 minutes. We observed that DHPG caused LTD of fEPSP responses in WT slices that was exaggerated in the hippocampus of GluN2B^{2ACTD} mice (**Fig. 4G**). In contrast, the magnitude of mGluR-LTD was significantly reduced in GluN2A^{2BCTD} mice (**Fig. 4H**)**.** Thus, GluN2B^{2ACTD} and GluN2A^{2BCTD} show mirror opposite alterations in mGluR-LTD relative to WT littermates, reminiscent of findings observed in mouse models of FXS and TSC, respectively. The finding that the maximal transient depression immediately following application of DHPG did not differ between GluN2 CTD genotypes suggests that these findings are unlikely to be accounted for by differences in mGluR$_5$ expression[48].

Loss of mNMDAR signaling promotes epileptogenesis in the hippocampus

Previous studies have shown that elevation of basal protein synthesis can lead to epileptogenesis within area CA3 of the hippocampus[49]**,** which can be mimicked by stimulating mGluR$_{1/5}$ with DHPG**.** To examine whether the GluN2 CTD modulates excitability, we placed a recording electrode in the

pyramidal layer of CA3 in transverse hippocampal slices from GluN2B^{2ACTD}, GluN2A^{2BCTD}, and WT littermates. Slices were perfused with ACSF for 10 minutes to obtain a baseline before we monitored spontaneous and epileptiform activity in response to the $GABA_A$ antagonist bicuculline (50 μM) or DHPG (50 μM), respectively (**Fig. 5A**). In control slices, addition of bicuculline led to short, rhythmic, ictal-like events of <1.5 seconds (**Fig. 5B$_i$**). However, in the presence of DHPG ictal-like events progressed to prolonged synchronized discharges (**Fig. 5B$_{ii}$**). Intriguingly, in slices from GluN2B^{2ACTD} mice, $GABA_A$ blockade alone led to a dramatic increase in burst duration and frequency (**Fig. 5C$_i$**), similar to the effect of DHPG (**Fig. 5C$_{ii}$**). In GluN2A^{2BCTD} slices, however, bicuculline had a similar effect to that seen in WT slices (**Fig. 5D-E$_i$**) and DHPG failed to induce short or long duration events (**Fig. 5D-E$_{ii}$**). Therefore, replacing the GluN2A CTD with the GluN2B CTD blocks $mGluR_{1/5}$-induced epileptogenesis. Together these data suggest that switching the GluN2 CTD leads to a hyper- and hypo- sensitive response to $mGluR_{1/5}$ activation in GluN2B^{2ACTD} and GluN2A^{2BCTD} slices, respectively.

Switching the GluN2A C-terminal domain with GluN2B normalizes protein synthesis and mGluR-LTD in the *Fmr1* KO mouse

Based on these findings, it appears that GluN2B CTD expression strongly modulates functions related to $mGluR_5$-dependent protein synthesis (**Fig. 6A**). Deleting the GluN2B CTD in GluN2B^{2ACTD} mice exacerbates phenotypes downstream of $mGluR_5$ activation, while genetically enhancing the expression of GluN2B CTD suppresses $mGluR_5$-dependent phenotypes in the hippocampus. As there are numerous reports that $mGluR_5$ contributes to disease phenotypes in the mouse models of ID[27,28,50], we wanted to explore whether manipulating mNMDAR signaling in the *Fmr1* KO mouse could correct some of the core phenotypes in FXS**.** We introduced the GluN2A^{2BCTD} mutation into *Fmr1* KO mice by crossing *Fmr1* heterozygous females with GluN2A^{2BCTD} heterozygous males to enhance mNMDAR signaling (**Fig. 6B**), and measured protein synthesis in the progeny. The results reveal that elevated protein synthesis in *Fmr1* KO mice is significantly reduced to WT levels by switching the CTD of GluN2A with GluN2B (**Fig. 6C**).

The correction of protein synthesis with the introduction of the GluN2A^{2BCTD} knockin mutation led us to speculate that other pathological phenotypes could be reversed by augmenting GluN2B signaling in *Fmr1* KO mice. To examine this, we measured mGluR-LTD in the *Fmr1* KO x GluN2A$^{(2BCTD)}$ cross. Consistent with previous studies, the acute application of DHPG (50 μM, 5 mins) revealed that mGluR-LTD is exaggerated in *Fmr1* KO mice relative to WT littermates (**Fig. 6D**). The GluN2A$^{(2BCTD)}$ heterozygous mutation led to a small but significant suppression of mGluR-LTD when compared to WT mice (**Fig. 6E**). Importantly, the *Fmr1* KO x GluN2A^{2BCTD} cross exhibits a magnitude of LTD indistinguishable from WT mice (**Fig. 6F**). Together, our results show that the enhancement of GluN2B CTD expression through the introduction of the GluN2A^{2BCTD} mutation is

sufficient to correct excessive protein synthesis and exaggerated mGluR-LTD in the *Fmr1* KO hippocampus.

Dysregulated protein synthesis and audiogenic seizures in *Fmr1* KO mice are corrected by modulating GluN2B.

Previous studies in *Fmr1* KO mice have shown that correction of altered protein synthesis is highly predictive of improvements in structural, circuit, and behavioral phenotypes[28,43,50,51]. According to our model, augmenting GluN2B signaling should ameliorate FXS phenotypes. Glyx-13 has recently been shown to preferentially target GluN2B containing receptors at an allosteric site distinct from the glutamate and glycine binding sites[52,53]. Furthermore, it is known to be a cognitive enhancer in several learning and memory paradigms[54-56]**.** To test the potential utility of augmenting NMDAR function in fragile X, we treated *Fmr1* KO and WT hippocampal slices with Glyx-13 (0.1 μM) and measured protein synthesis levels (**Fig. 7A**). Once again, we observed a significant increase in ^{35}S incorporation in *Fmr1* KO slices relative to WT littermates under basal conditions. Importantly, pretreatment with Glyx-13 normalized excessive protein synthesis in *Fmr1* KO mice to WT levels under these conditions (**Fig. 7B**). This result supports the hypothesis that positively modulating GluN2B under tonic conditions corrects one of the core deficits in *Fmr1* KO hippocampus.

In addition to an increase in spine density and hyperexcitability within the hippocampal circuit, another consequence of altered protein synthesis in *Fmr1* KO mice is enhanced susceptibility to audiogenic seizures (AGS)[28,50,51]. Encouraged by our initial findings we next wanted to determine whether Glyx-13 could reduce the incidence of AGS in *Fmr1* KO mice *in vivo. Fmr1* KO and WT littermates (P19-25) mice were injected with either saline or Glyx-13 (1 mg/kg). After 1 hr, mice were transferred to a chamber and habituated for 1 minute before they were exposed to a 120dB stimulus for 2 minutes (**Fig. 7C**). As expected, saline-treated *Fmr1* KO mice exhibited an increased susceptibility to seizures relative to WT littermates (**Fig. 7D, E**). However, a single dose of Glyx-13 was able to significantly reduce seizure susceptibility in *Fmr1* KO mice, without impacting the incidence of seizures in WT mice. These findings further support the hypothesis that positively modulating GluN2B signaling can rescue both i*n vitro* and *in vivo* phenotypes in *Fmr1* KO mice.

DISCUSSION

The current study reveals that GluN2B is necessary and sufficient for mNMDAR signaling in the absence of ion flux, and that this signaling can mitigate core fragile X phenotypes linked to altered protein synthesis regulation. In addition, the data clarify the roles of GluN2A and GluN2B subunits in initiating NMDAR-dependent LTD and structural plasticity in CA1.

NMDAR molecular motifs involved in non-ionotropic structural and ionotropic functional plasticity in CA1

We have previously shown that changes in the length and volume of dendritic spines in response to NMDA proceeds independently of ion flux and is dependent on mTORC1 and *de novo* protein synthesis[24]. Conversely, LTD of synaptic transmission initiated by NMDA occurs in the absence of mTORC1 activity or new protein synthesis but requires ion flux through the receptor channel. In the current study we find that structural and functional plasticity in CA1 can be further dissociated by their dependence on GluN2 subunits. LTD, as measured by a change in synaptic transmission evoked by stimulation of the Schaffer collateral pathway, requires ligand binding to GluN2B but is also sensitive to genetic and pharmacological inhibition of GluN2A. Conversely, non-ionotropic signaling as reported by spine shrinkage is solely dependent on receptors containing GluN2B. We note that these conclusions explicitly apply to ages and experimental conditions when LTD depends on ion flux through the NMDARs and may differ during early development[21].

We found that pharmacologically limiting ion flux through GluN2A-containing assemblies, or deleting the *Grin2A* gene (constitutively or conditionally), reduces the magnitude of NMDAR-LTD. However, LTD was fully abolished only when the LBD of GluN2B was blocked. Combined, these data suggest that both the GluN2B/GluN1 di-heteromeric and GluN2A/GluN2B/GluN1 tri-heteromeric assemblies contribute to LTD at CA1 synapses, whereas GluN2A/GluN1 di-heteromeric receptors do not. The GluN2B subunit is also crucial for non-ionotropic signaling reported as spine shrinkage. Structural plasticity was eliminated by antagonizing the LBD of GluN2B, genetically deleting this receptor subunit, or swapping out its CTD. Indeed, because deletion of GluN2A has no quantitative effect on spine shrinkage in response to NMDA, the data suggest that the GluN2B di-heteromeric receptors can account for the full effect of mNMDAR signaling.

Previous work has implicated CAMKII, p38 MAPK and neuronal nitric oxide synthase signaling in driving actin depolymerisation and the retraction of dendritic spines[10,12] as well as gating LTP-associated spine growth associated with long-term potentiation[13]. Our results indicate that GluN2B di-heteromeric assemblies are sufficient to support spine shrinkage caused by mNMDAR activation, and that the GluN2B LBD and CTD are critical structural motifs. Considered with the previous study by Thomazeau et al (2020), who also used NMDA to trigger spine shrinkage, the data indicate that GluN2B signals through mTORC1 to modulate protein synthesis that serves as a gate for structural plasticity.

How might the GluN2B CTD mediate its non-ionotropic functions and couple to downstream pathways controlling spine morphology and translation? Biochemical and genetic studies have demonstrated that the GluN2B CTD plays an essential role in the supramolecular assembly of NMDARs with scaffold proteins and signaling enzymes, which are key regulators of structural and functional plasticity[57]. GluN2B di- and tri-heteromers assemble into 1.5 MDa supercomplexes whereas GluN2A di-heteromers can only assemble into 0.8 MDa complexes lacking MAGUKs and signaling molecules. Thus, the physiological functions observed for the GluN2B CTD could arise

from its role in positioning of the receptor with its effector proteins and/or direct regulation of the signaling complex.

Although GluN2A signaling appears to be unnecessary for triggering spine shrinkage, there is evidence for non-ionotropic signaling by GluN2A/GluN1 diheteromeric NMDARs leading to tyrosine dephosphorylation of the GluN2A subunit[58]. Similarly, in HEK293 cells expressing GluN2A/GluN1 and in cultured cortical neurons, it has been reported that glycine triggers non-ionotropic signaling that confers neuroprotection [59]. These and related studies indicate that non-ionotropic NMDAR signaling is multifaceted and not restricted to the regulation of spine structure by GluN2B in the hippocampus[18,60].

Regulation of protein synthesis by mNMDAR signaling

Further examination of mNMDAR signaling reveals that the GluN2B subtype can bidirectionally regulate protein synthesis. Brief NMDA application reduces bulk protein synthesis, and antagonizing the NMDAR LBD under basal conditions causes a significant elevation. Importantly, modulation of translational rates occurs in the presence of the channel blocker MK-801, suggesting that non-ionotropic mNMDAR signaling represents an important pathway by which synaptic activity regulates protein synthesis.

Consistent with this conclusion, we find that augmenting mNMDAR signaling by replacing the GluN2A CTD with the GluN2B CTD mimics the effect of agonist application on protein synthesis in WT hippocampus. Conversely, elimination of mNMDAR signaling by swapping out the GluN2B CTD mimics the effect of D-AP5 on WT protein synthesis. The functional significance of protein synthesis modulation by mNMDAR signaling through GluN2B is suggested by the impact on LTD induced by activating $mGluR_{1/5}$ with DHPG[47]. In the age range examined in this study, DHPG stimulates new protein synthesis that is required for induction of mGluR-LTD in WT mice [28,44,47,61]. DHPG-induced mGluR-LTD is augmented in slices from $GluN2B^{(2ACTD)}$ mice with increased protein synthesis rates, and it is reduced in slices from $GluN2A^{(2BCTD)}$ mice with reduced basal protein synthesis. Going forward, it will be of great interest to investigate how the well-known effects of age and sensory experience on NMDAR subunit composition impact protein synthesis regulation and its functional consequences during development[62].

Our findings of reduced global protein synthesis in response to mNMDAR activation are consistent with earlier reports in cortical cultures which demonstrated that the GluN2B subunit suppresses protein synthesis[63,64]. Interestingly, global protein synthesis is also reduced in a mouse model of tuberous sclerosis in which mTORC1 signaling is hyperactive[42]. In this case, suppression of overall protein synthesis reflects a decrease in translation of terminal oligopyrimidine (TOP) containing mRNA transcripts and an increase in FMRP-binding targets that tend to encode large synaptic proteins[65]. When considered with the finding that mNMDAR-induced structural plasticity is blocked by the mRNA translation inhibitor cycloheximide, these results suggest that GluN2B triggers

a shift in the translation pool rather than stalling mRNA translation *per se*. Based on these findings, we propose that agonist binding to the GluN2B LBD triggers a conformational change in the CTD of GluN2B di-heteromers to activate mTORC1 signaling and initiate mRNA translation and the synthesis of proteins that support the depolymerisation of the actin cytoskeleton and the retraction of dendritic spines. It will be of great interest to identify actively translating mRNAs downstream of non-ionotropic mNMDAR signaling and understand how they contribute to structural plasticity at CA1 synapses.

Mimicry and correction of core cellular phenotypes in *Fmr1* KO mice

Recently, it has been reported that elevated protein synthesis in *Fmr1* KO mice reflects a length-dependent shift in the translating pool of mRNAs[66]. There is an over-translation of short mRNA transcripts encoding ribosomal proteins at the expense of longer mRNAs encoding synaptic proteins and FMRP targets. Consequently, synaptic and circuit plasticity that is normally dependent on *de novo* protein synthesis are disrupted in the *Fmr1* KO and persist in the presence of protein synthesis inhibitors[24,45,67]. We previously found that this also applies to NMDA-induced spine shrinkage in *Fmr1* KO mice, which unlike WT, proceeds in the presence of cycloheximide[24].

Here we show that replacing the GluN2B CTD with GluN2A, and thus eliminating mNMDAR signaling, leads to increased protein synthesis and spine density, exaggerated mGluR-LTD in CA1, and epileptiform activity in CA3. These differences in hippocampal structure and function phenocopy observations in the *Fmr1* KO mouse[27,51,68]. An exception is spine shrinkage in response to NMDA, which is absent in the B2A mice but present in *Fmr1* KO mice[24].
On the flip side, overexpression of the GluN2B CTD reduces both LTD and the increase in neuronal excitability triggered by $mGluR_{1/5}$ activation. Collectively, these data demonstrate that non-ionotropic mNMDAR signaling strongly modulates the intracellular consequences of activating $mGluR_{1/5}$, which have been linked to pathophysiology in several neurodevelopmental disorders that, in addition to fragile X, include tuberous sclerosis complex[42,69], *SYNGAP1* haploinsufficiency[46], Rett syndrome[70], chromosome 16p11.2 microdeletion syndrome[71], and autism[72].

Numerous prior studies have shown that selectively inhibiting $mGluR_5$ or its downstream signaling normalizes protein synthesis and rescues a multitude of synaptic and behavioral phenotypes in the *Fmr1* KO[73]. Similarly, enhancing mTORC1 signaling through the introduction of the *Tsc2* mutation corrects synaptic pathophysiology in FXS[42]. This motivated us to try and reverse the core pathophysiology associated with *Fmr1* KO mice, by increasingly mNMDAR signaling through the introduction of $GluN2A^{2BCTD}$ mutation. In the absence of FMRP, increasing the expression of the GluN2B CTD reduced exaggerated protein synthesis, mGluR-LTD, and epileptiform activity in the hippocampus of *Fmr1* KO mice.

Allosteric augmentation of mNMDARs, in principle, could improve synaptic regulation of mTORC1 and by doing so restore the normal balance of high- and low-efficiency mRNA translation in fragile X[74,75]. In a preliminary test of this hypothesis, we observed that Glyx-13, a positive modulator of NMDARs[55,76], corrected the protein synthesis phenotype in *Fmr1* KO hippocampus. Encouraged by these findings, we also investigated the consequence of modulating NMDARs on audiogenic seizures, an *in vivo* phenotype in *Fmr1* KO mice that is associated with altered protein synthesis regulation[77]. A single dose of Glyx-13[78] was sufficient to significantly reduce the incidence of seizures. Glyx-13 acts on NMDARs at an allosteric site distinct from the glutamate and glycine binding sites[52]. It remains to be determined if the effect of this compound on AGS is independent of effects on NMDAR ion flux.

Mutations in GluN2B have been linked to numerous types of epilepsy including epileptic encephalopathies, focal epilepsy, partial seizures and infantile spasms[79-81]. In addition, deletion of GluN2B leads to an increase in the number of excitatory inputs on to pyramidal neurons in the prefrontal cortex[64]. In the current study we also detected an increase in CA1 spine density in the absence of the GluN2B CTD and, in CA3, we find prolongation of epileptiform bursts in response to $mGluR_{1/5}$ activation. Together, these findings demonstrate that the GluN2B subunit makes a critical contribution to circuit refinement, protein synthesis regulation, and circuit excitability in the juvenile hippocampus. Identifying compounds that can selectively modulate this unique mode of signaling may prove to be a highly valuable target in treating neurodevelopmental disorders.

Limitations of the study

Most of our experiments were performed in mice between P25 and 35 to be consistent with previous work[24]. We also examined NMDA-induced spine shrinkage, in the presence of MK-801, in a small cohort of mice ≥ P60 and observed that NMDA induces a reduction in spine volume (83 ± 1.7%, $n = 3$), similar in magnitude to what is observed in mice between the ages of P25-35. This is not surprising given that GluN2B remains the dominant subtype, even as GluN2A expression levels rise from P14 [40,82]. Nevertheless, we cannot rule out the possibility that the signaling requirements for mNMDAR signaling may be different in fully mature hippocampal synapses. This will require further study.

In numerous prior studies, it has been shown that varied approaches that correct the aberrant protein synthesis in *Fmr1* KO (e.g., $mGluR_5$ NAMs, lovastatin, metformin, GSK3 inhibitors) all similarly, and without exception, rescue an array of electrophysiological and behavioral phenotypes that include inhibitory avoidance deficits and audiogenic seizures[73]. Some of these have been examined in the current study (mGluR-LTD and CA3 excitability). Although behavioral phenotypes were not studied in *Fmr1* KO x $GluN2A^{2BCTD}$ double mutants, we did show that an NMDAR PAM, Glyx-13, rescues the seizure phenotype in the *Fmr1* KO. It will be of great interest to examine the

effects of modulating of mNMDAR signaling on additional behavioral phenotypes in the *Fmr1* KO in future studies.

Bulk protein synthesis is reduced by mNMDAR activation in WT mice (**Fig. 4D**). The findings that protein synthesis is elevated by the competitive LBD inhibitor D-AP5 in WT mice (**Fig. 4C**), and in mice lacking the GluN2B CTD (**Fig. 4E**), suggest that there is constitutive activity in the absence of synaptic stimulation. Consistent with this interpretation, we find that replacing the GluN2A CTD with the GluN2B CTD, which presumably augments this constitutive signaling, also reduces bulk protein synthesis to levels comparable to those observed in WT when stimulated with NMDA (**Fig. 4F**). However, we did not perform the basal protein synthesis measurements in the presence of MK-801 in the A2B mice and therefore cannot rule out an additional contribution of ionotropic signaling to this decrease[62,83,84]. It would be interesting to know whether additional stimulation with NMDA in the A2B mice would further suppress protein synthesis beyond the constitutive reduction.

Many studies have used selective agonists such as NMDA and DHPG to induce plasticity in the hippocampal slice. The advantage of this method is that it elicits changes at a large population of Schaffer collateral synapses, not just those activated by a stimulating electrode, and this enables coordinated biochemical, structural and electrophysiological analysis of synaptic plasticity. Agonist induced mGluR- and NMDAR-dependent LTD occludes and is occluded by LTD induced with electrical stimulation, indicating a shared expression mechanism[4,47,85]. Although similar occlusion experiments have not been performed with structural plasticity, it has been shown that spines shrink in response to glutamate uncaging at individual synapses[86] and these changes are triggered by non-ionotropic activation of NMDARs[87]. It therefore seems very likely that the conclusions of our study apply regardless of the route of induction, but this should be confirmed in future studies.

A strength of this study is the use of multiple approaches to confirm our conclusions. A case in point is the conclusion that activation of GluN2B is necessary and sufficient to account for the mNMDAR signaling leading to spine shrinkage. It is *necessary*, because spine changes in response to NMDA are eliminated by genetic deletion of GluN2B (**Fig. 1E**), pharmacological blockade of the ligand binding site on GluN2B (**Fig. 2C**), and by replacing the GluN2B CTD (**Fig. 3E**). It is *sufficient* because there is no effect of genetic elimination of GluN2A (**Fig. 1Aii**), pharmacological inhibition of GluN2A (**Fig. 2Eii**), or replacing the GluN2A CTD (**Fig. 3B**). Although it was not an explicit aim of this study, our experiments also shed light on the contributions of GluN2A and GluN2B subunits on functional LTD induced by NMDA. The finding that selective inhibition of ligand binding to GluN2B with Conantokin-G (2 μM)[88] eliminated LTD suggests that GluN2A di-heteromeric receptor activation is not sufficient to support induction (**Fig. 2C**). Similarly, although residual LTD is observed in the GluN2A knockout (**Fig. 1A**), it does not appear that GluN2B di-heteromeric receptors are necessary as LTD is unaffected by 30 μM Ro25-6891, a GluN2B negative allosteric modulator that preferentially targets these receptors[39] (**Supplemental Fig. 1**). Our data support the notion that

the primary trigger for LTD is activation of GluN2A/B tri-heteromeric receptors which have been shown to contribute 50% or more of the ion flux triggered by synaptic activation of NMDARs in CA1[39,89]. These receptors are strongly inhibited by Conantokin-G[88] whereas ion flux through them is only partially inhibited by MPX-004 (30 μM)[36], paralleling the effects of these compounds on LTD (**Fig. 2C, E**). This conclusion is provisional, however, as further work is required to fully characterize the selectivity and potency of the compounds used in our study.

Figure Legends

Figure 1: **Spine structural plasticity triggered by non-ionotropic NMDAR signaling depends on the GluN2B subunit**. (**A**$_{i\text{-}ii}$) Extracellular field recordings and time-lapse two-photon imaging were simultaneously performed in CA1 stratum radiatum of acute hippocampal slices prepared from *Grin2A* KO Thy1-GFP mice and WT littermates. Representative fEPSP traces and images are shown 15 mins before, 15 mins and 60 mins after LTD induction. NMDA infusion occurred during the time indicated by the orange shading. (**A**$_i$) Brief bath application of NMDA (20 μM; 3 mins) induces a persistent reduction in the slope of the fEPSP in WT Thy1-GFP slices that is significantly impaired in *Grin2A* KO Thy1-GFP slices (WT: 35 ± 6%, n = 8; *Grin2A* KO: 62 ± 5%, n = 5; p = 0.01, unpaired t-test). (**A**$_{ii}$) In contrast, NMDA triggered a decrease in spine volume in WT Thy1-GFP slices which persisted in the absence of the *Grin2A* allele (WT: 84 ± 2%, n = 8; *Grin2A* KO: 85 ± 5%, n = 5; p = 0.87, unpaired t-test) indicating that the GluN1/GluN2B di-heteromeric receptors are sufficient to support mNMDAR signaling. (**B**) Schematic of HSV injections into the dorsal hippocampus of floxed *Grin2A* and *Grin2B* mice created with Biorender.com. (**C**) Experimental timeline of conditional knockout (cKO) of *Grin2A* and *Grin2B* in the dorsal hippocampus of floxed *Grin2A* and *Grin2B* mice through injections of either HSV-eGFP control or HSV-eGFP-Cre. (**D**) Conditional deletion of the *Grin2A* gene has no effect on structural plasticity in response to NMDAR activation (HSV Control: 87 ± 5%, n = 4; HSV-Cre-*Grin2A* cKO 83 ± 1%, n = 7; p = 0.36, unpaired t-test). (**E**) Loss of *Grin2B* significantly impairs NMDA-induced spine shrinkage (HSV Control: 86 ± 3%, n = 6; HSV-Cre-*Grin2B* cKO: 97 ± 2%, n = 10; p = 0.0097, unpaired t-test).

Figure 2: **Pharmacology of NMDAR-mediated functional and structural plasticity indicates that agonist binding to GluN2B is critical**. (**A**) Schematic of the predominant NMDAR assemblies in hippocampal CA1 and binding sites for GluN2A and GluN2B subtype-selective compounds. The GluN2B competitive antagonist Conantokin-G (Con-G) blocks the glutamate binding site on 2A/2B tri-heteromers and 2B di-heteromers. The negative allosteric modulator (NAM) of GluN2A MPX-004 binds to the N-terminal domain (NTD) of 2A di-heteromers and 2A/2B tri-heteromers. (**B**) Con-G (2 μM) eliminated 66% of the isolated NMDAR-mediated fEPSP (WT vehicle: 100 ± 14%; WT Con-G: 34 ± 6%, n = 15; p = 0.00016, unpaired t-test), abolished both NMDA-induced LTD (**C**$_i$; WT vehicle: 46 ± 6%, n = 8; WT Con-G: 108 ± 3%, n = 10; p < 0.0001, unpaired t-test) and spine shrinkage at CA1 synapses (**C**$_{ii}$; WT vehicle: 85 ± 3%, n = 8; WT Con-G: 96 ± 1%, n = 9; p = 0.002, unpaired t-test). (**D**) MPX-004 (30 μM) caused a 47% block of the isolated NMDAR-fEPSP (WT vehicle: 100 ± 13%; WT MPX-004: 53 ± 4%, n = 14; p = 0.0013, unpaired t-test) and a comparable inhibition of

LTD (**Ei**; WT vehicle: 46 ± 7%, *n* = 11; WT MPX-004: 75 ± 11%, *n* = 13; *p* = 0.03; unpaired *t*-test), but had no effect on spine shrinkage (**Eii**; WT vehicle: 87 ± 3%, *n* = 11; WT MPX-004: 89 ± 3%, *n* = 13; *p* = 0.64, unpaired *t*-test). Representative fEPSP traces and images in panels **C** and **E** are shown 15 mins before, 15 mins and 60 mins after LTD induction.

Figure 3: Non-ionotropic **NMDARs induce spine shrinkage through the GluN2B carboxyl terminal domain**. (**A**, **D**) Schematic of genetically engineered GluN2A^{2BCTD} (termed A2B) and GluN2B^{2ACTD} (termed B2A) knock-in mouse lines where the exon encoding the CTD of GluN2A is deleted and replaced with GluN2B (A2B) and vice versa (B2A). (**B**, **C**) Introduction of the GluN2B CTD on GluN2A-containing receptors has no significant effect on NMDA-induced structural plasticity (WT: 80 ± 2%, *n* = 4; GluN2A^{2BCTD} HOM: 81 ± 3%, *n* = 6; *p* = 0.96, unpaired *t*-test) or spine density along apical dendrites of CA1 pyramidal neurones (WT: 4.60 ± 0.64, *n* = 5; GluN2A^{2BCTD} HOM: 4.20 ± 0.21, *n* = 6; *p* = 0.25, unpaired *t*-test). (**E, F**) Switching the GluN2B CTD with 2A leads to a significant impairment in NMDA-induced structural plasticity (WT: 81 ± 3%, *n* = 4, GluN2B^{2ACTD} HOM: 96 ± 2%, *n* = 6, *p* = 0.005, unpaired *t*-test) and a modest increase in spine density in B2A homozygous mice relative to WT littermates (WT: 3.96 ± 0.20, *n* = 5, GluN2B^{2ACTD} HOM: 4.72 ± 0.20, *n* = 7; *p* = 0.029, unpaired *t*-test). Representative images in panels **B** and **E** are from 15 mins before, 15 mins and 60 mins after LTD induction.

Figure 4: Non-ionotropic NMDAR signaling through the GluN2B CTD negatively regulates bulk protein synthesis and mGluR-LTD. (**A**) Experimental timeline for measuring protein synthesis in acute hippocampal slices. Transverse hippocampal slices were recovered for 4 hrs in ACSF before transcription was blocked with actinomycin D (25 μM) ± drug, and newly synthesized proteins radiolabeled with ^{35}S methionine/cysteine (10 μCi/mL) ± drug. (**B**) The acute application of NMDA (20 μM, 3 mins) leads to a significant decrease in the ^{35}S incorporation relative to vehicle-treated slices (vehicle: 100 ± 5%; NMDA: 79 ± 6%; *n* = 8, *p* = 0.014, paired *t*-test). (**C**) In contrast, the non-selective, competitive antagonist D-APV (50 μM) causes a significant increase in protein synthesis in hippocampal slices (vehicle: 100 ± 4%; D-APV: 117 ± 6%; *n* = 12, *p* = 0.046, paired *t*-test). (**D**) The acute application of NMDA leads to a reduction in ^{35}S incorporation relative to vehicle treated slices that persisted in the presence of the NMDAR ion channel blocker MK-801 (vehicle: 100 ± 2%; NMDA: 75 ± 6%; MK-801: 97 ± 5%; NMDA/MK-801: 82 ± 5%; *n* = 7, *p* = 0.0018, ANOVA). (**E**) Metabolic labeling reveals bulk protein synthesis is elevated in GluN2B^{2ACTD} (B2A) mice compared to WT littermates (WT: 100 ± 2%, *n* = 13; B2A HET: 116 ± 5%, *n* = 7; B2A HOM: 113 ± 4%, *n* = 8; *p* = 0.0051, ANOVA). (**F**) Metabolic labeling of hippocampal slices reveals the genetic introduction of GluN2B CTD into the GluN2A locus (GluN2A^{2BCTD}; A2B) reduces protein synthesis in a gene dose-dependent manner (WT: 100 ± 2%, *n* = 13; A2B HET: 91 ± 3% *n* = 15; A2B HOM: 79 ± 3%, *n* = 15; *p* < 0.0001, ANOVA). (**G**) The acute of application of the group 1 mGluR$_{1/5}$ agonist DHPG (50

μ M, 5 mins) induces a long-lasting depression of fEPSPs in CA1 of the hippocampus. Representative fEPSP traces are shown at 15 mins before and 60 mins after LTD induction. Replacing the GluN2B CTD with GluN2A significantly enhanced mGluR-LTD in B2A mice relative to WT littermates (WT: 83 ± 5 %, n = 7; B2A HOM: 65 ± 4%, n = 6; p = 0.017, unpaired t-test). (**H**) In contrast, mGluR-LTD is inhibited in the hippocampus of A2B mice relative to WT littermates (WT: 80 ± 2 %, n = 6; A2B HOM: 104 ± 4%, n = 5; p = 0.0008, unpaired t-test).

Figure 5: Enhancing or eliminating mNMDAR signaling by switching the GluN2 CTD bidirectionally regulates CA3 epileptogenesis. (**A**) Experimental timeline for extracellular recordings in hippocampal CA3. Transverse hippocampal slices were recovered before a recording electrode was placed in the pyramidal layer of CA3. Slices were perfused with ACSF for 10 mins before being treated with either the $GABA_A$ receptor antagonist bicuculline (Bic, 50 μM) or the group 1 mGluR agonist DHPG (50 μM) for 1 hr. (**B_i**) Extracellular recordings in CA3 pyramidal cell layer of WT hippocampal slices perfused with ACSF containing bicuculline primarily generates short rhythmic events (short events <1.5s = 517, long events ≥1.5s = 88, average burst duration of 605 events = 1.23 ± 0.04s, n = 8). (**B_{ii}**) Bath application of DHPG generates significantly longer burst events (short events <1.5s = 192, long events ≥1.5s = 80, average burst duration of 272 events = 1.76 ± 0.10s, n = 11, p < 0.0001 ANOVA). (**C_i**) $GABA_A$ blockade with bicuculline triggers a greater number of epileptiform discharges that are longer in burst duration in CA3 region of hippocampal slices from $GluN2B^{2ACTD}$ (B2A) mice compared to WT mice (B2A: short events <1.5s = 697; long events ≥1.5s = 243, average burst duration of 940 events = 1.88 ± 0.07s, n = 7, p < 0.0001, ANOVA). (**C_{ii}**) Similarly, burst frequency and duration are increased in B2A slices perfused with DHPG compared to WT mice (B2A: short events <1.5s = 613; long events ≥1.5s = 407, average burst duration of 1020 events = 1.83 ± 0.05s, n = 7, p < 0.0001, ANOVA). (**D_i**) WT hippocampal slices perfused with ACSF containing bicuculline primarily generates short rhythmic events (bicuculline: short events <1.5s = 289, long events ≥1.5s = 5, average burst duration of 294 events = 1.04 ± 0.01s, n = 9). (**D_{ii}**) Bath application of DHPG generates short rhythmic events that lead to an increase in prolonged discharges (DHPG: short events <1.5s =136, long events ≥1.5s = 54, average burst duration of 190 events = 1.42 ± 0.07s, n = 10) (**E_i**) Bicuculline induces comparable short and long events in $GluN2A^{2BCTD}$ (A2B) mice compared to WT littermates (A2B: short events <1.5s = 253; long events ≥1.5s = 3, average burst duration of 256 events = 1.03 ± 0.01s, n = 8). (**E_{ii}**) DHPG can no longer induce short or prolonged discharges in A2B hippocampal slices (A2B: short events <1.5s = 0; long events ≥1.5s = 0, n = 7). All scale bars 30s, 50 mV.

Figure 6: **Increasing the expression of GluN2B C-terminal domain normalizes protein synthesis and mGluR-LTD in the *Fmr1* KO mouse**. (**A**) Schematic depicting the inverse relationship between GluN2B CTD expression and $mGluR_5$ function. (**B**) Genetic rescue strategy in which *Fmr1*

heterozygous females are crossed with male GluN2A^{2BCTD} (A2B) heterozygous mice to produce male offspring of four genotypes: wild-type (WT), *Fmr1* KO (KO), A2B het (A2B), and *Fmr1* KO/A2B het cross (CR). (**C**) Replacing the C-terminal domain of GluN2A with GluN2B in *Fmr1* KO reduces elevated protein synthesis rates in the hippocampus (WT: 100 ± 3%, n = 21; *Fmr1* KO: 114 ± 5%, n = 11; A2B HET: 97 ± 3%, n = 13 Cross: 89 ± 3%, n = 14; ANOVA A2B genotype p = 0.0002). (**D**) The magnitude of DHPG-induced mGluR-LTD (50 µM, 5 mins) in hippocampal CA1 is exaggerated in *Fmr1* KO mice relative to WT littermates (WT: 85 ± 3%, n = 10; *Fmr1* KO: 70 ± 6%, n = 10; unpaired t-test, p = 0.029). (**E**) In contrast, mGluR-LTD is significantly impaired in GluN2A$^{(2BCTD)}$ heterozygote mice (WT: 85 ± 3%, n = 10; A2B: 98 ± 3%, n = 8, unpaired t-test, p = 0.013). (**F**) Introduction of the GluN2A$^{(2BCTD)}$ mutation in *Fmr1* KO mice restores elevated mGluR-LTD to WT levels (WT: 85 ± 3%, n = 10; Cross: 85 ± 4%, n = 9, unpaired t-test, p = 0.99). (**G**) Comparison of all four genotypes reveals a suppressive effect of the GluN2A$^{(2BCTD)}$ heterozygous mutation, lowering mGluR-LTD in the *Fmr1* KO hippocampus to WT levels (ANOVA A2B/*Fmr1* genotype p = 0.003).

Figure 7: Dysregulated protein synthesis and audiogenic seizures in *Fmr1* KO mice are corrected by modulation of mNMDAR signaling. (**A**) Experimental timeline for metabolic labeling in the presence of the NMDA partial agonist Glyx-13. (**B**) Glyx-13 (0.1 µM) restored elevated protein synthesis in *Fmr1* KO mice to WT levels (WT vehicle: 100 ± 6%; KO vehicle: 118 ± 5%; WT Glyx-13: 99 ± 7%; KO Glyx-13: 94 ± 5%; ANOVA p = 0.034, n = 8). (**C**) Experimental timeline for the *in vivo* treatment of WT and *Fmr1* KO mice with Glyx-13 (1 mg/kg) prior to audiogenic seizure (AGS) testing. Mice were injected with either saline or Glyx-13 (1 mg/kg) 1 hr prior to AGS testing. Seizures were scored for wild running, clonic seizure, tonic seizure and death. (**D, E**) AGS incidence is significantly increased in saline treated *Fmr1* KO mice relative to WT littermates (WT saline: 13%, n = 15; KO saline: 82%, n = 11; Fisher's exact test p = 0.0009). Treatment with Glyx-13 had no effect on the incidence of seizures in WT mice, but significantly reduced AGS incidence in *Fmr1* KO mice (WT Glyx-13: 14%, n = 14; KO Glyx-13: 31%, n = 16, Fisher's exact test p = 0.018).

Supplemental Figure 1: NMDA-induced LTD and spine shrinkage is unaffected by negative allosteric modulation of the GluN2B N-terminal domain. The negative allosteric modulator Ro25-6981, targets the N-terminal domain of GluN2B containing NMDARs, limiting ion flux through the receptor. (**A**) Ro25-6981 (30 µM) eliminated 51% of the isolated NMDAR-mediated fEPSP (WT vehicle: 100 ± 10%; WT Ro25-6981: 49 ± 7%, n = 8; p = 0.0010, unpaired t-test) but had no effect on either LTD (**Bi**; WT vehicle: 21 ± 5%, n = 8; WT Ro25-6981: 15 ± 3%, n = 8; p = 0.225, unpaired t-test) or spine shrinkage (**Bii**; WT vehicle: 90 ± 3%, n = 8; WT Ro25-6981: 89 ± 4%, n = 8; p = 0.95, unpaired t-test). Representative fEPSP traces and images are shown 15 mins before, 15 mins and 60 mins after LTD induction.

STAR★Methods

Key resources table

REAGENT or RESOURCE	SOURCE	IDENTIFIER
Antibodies		
Bacterial and virus strains		
ST HSV-cre-eGFP	Rachael Neve, Massachusetts General Hospital Gene Delivery Technology Core	RN5
ST HSV-eGFP	Rachael Neve, Massachusetts General Hospital Gene Delivery Technology Core	RN1
Biological samples		
Chemicals, peptides, and recombinant proteins		

NMDA	Sigma-Aldrich	M3262
Picrotoxin	Sigma-Aldrich	P1675
NBQX	Sigma-Aldrich	N183/1044
Glycine	Sigma-Aldrich	G7126
Conantokin-G	Tocris	4136
MPX-004	Alomone	M-280
Ro25-6981	Tocris	1594
D-AP5	Tocris	0106
Bicuculline	Sigma	14343
Actinomycin D	Tocris	1229
DHPG (U.of.E)	Sigma-Aldrich	D3689
DHPG (M.I.T)	Tocris	0805
MK-801	Sigma-Aldrich	M107
Glyx-13	Tocris	3406
Critical commercial assays		
DC Protein Assay kit II	Bio-Rad	5000112
EasyTag EXPRESS 35S Protein Labeling Kit	PerkinElmer	NEG772014MC
Deposited data		
Experimental models: Cell lines		
Experimental models: Organisms/strains		
Mouse: Thy1-GFP	The Jackson Laboratory	011070; RRID:IMSR_JAX:011070

	Feng et al. [90]	
Mouse: Grin2Afl/fl Grin2Bfl/fl	Gray et al. [33]	N/A
Mouse: GluN2A KO	Townsend et al. [91]	N/A
Mouse: Grin2A(2BCTD) Grin2B(2ACTD)	Ryan et al. [40]	N/A
Mouse: Fmr1 KO	The Jackson Laboratory	003025; RRID:IMSR_JAX:003025
Oligonucleotides		
Recombinant DNA		
Software and algorithms		
Graphpad Prism 9.0	GraphPad	
ImageJ	Schneider et al.	https://imagej.nih.gov/ij/
PClamp10	Axon Instruments	N/A
MATLAB R2023a	MathWorks	N/A
Microsoft Excel	Microsoft Office 2011	N/A
WinLTP 1999-2009	WinLTP Ltd., University of Bristol	N/A
Other		

Experimental model and study participant details

All mice were generated and/or bred for at least 6 generations on a C57BL6/J (003025) background obtained from The Jackson Laboratory. To generate GluN2A KO, Grin2A(^{2BCTD}) or Grin2B (^{2ACTD}) Thy1-GFP littermate pairs, the stock line was initially crossed with Thy1-GFP mice. Heterozygous progeny, for Thy1-GFP and mutant gene of interest, were used to breed experimental mice to produce WT and KO littermates for imaging experiments. Generation of double mutant lines involved crossing *Fmr1* heterozygous females with GluN2A$^{(2BCTD)}$ heterozygous males with only first-generation litters taken. Mice were group housed in non-environmentally enriched cages with unrestricted food and water access and a 12 h light-dark cycle. Experimental cohorts consisted of female and male littermates, except *Fmr1* KO lines, that were P25-35 at the time of experiments. All experiments were performed blind to genotype using age-matched littermate controls. At MIT, all animal care and procedures were approved by the MIT committee on Animal Care (CAC) and the Department of comparative medicine (DCM); they are also in compliance with the NIH "Guide for the care and use of laboratory animals". At the University of Edinburgh all animal husbandry was carried out by University of Edinburgh technical staff. All animal procedures were performed in accordance the regulations set by the University of Edinburgh and the UK Animals Act 1986.

Method details

CA1 viral infusions

Juvenile Grin2Afl/fl and Grin2B fl/fl mice (P25-30) were anaesthetized and received subcutaneous injections of preoperative analgesics (buprenorphine (0.1 mg/kg, meloxicam; 1 mg/kg, and 1% lidocaine) before being head-fixed on a stereotaxic frame. Craniotomies were performed over CA1 where 20 short pulses of 20 nl of herpes simplex virus (HSV) expressing

a cre-eGFP fusion protein (HSV-eGFP-cre) or HSV-eGFP as a control (~8.75×10^8 particles/ml) was injected at a rate of 43 nl/minute at 2-3 sites using a Nanoject III (Drummond Scientific) and a beveled glass injection pipette. After surgery mice received post-operative analgesics and were returned to their home cage. Around 5-7 days post injection, mice were sacrificed for recordings. Cre expression was generally limited to a sparse population of CA1 pyramidal cells in the dorsal hippocampus.

Preparation of Hippocampal Slices

Mice were anesthetized through isoflurane inhalation, sacrificed and hippocampi were isolated. At MIT, acute dorsal hippocampal slices (350 µm thick) were prepared using a vibratome (Leica Microsystems) in ice-cold dissection buffer containing (in mM): NaCl 87, sucrose 75, KCl 2.5, NaH_2PO_4 1.25, $NaHCO_3$ 25, $CaCl_2$ 0.5, $MgCl_2$ 7, ascorbic acid 1.3, and D-glucose 10, saturated with 95% O_2, 5% CO_2 (Sigma-Aldrich). For LTD and spine shrinkage experiments, the CA3 region was removed. Slices were initially recovered for 30 mins at 32.5 °C then at room temperature for 2.5 hrs in artificial cerebrospinal fluid (ACSF) containing (in mM): NaCl 124, NaH_2PO_4 1.2, KCl 5, $NaHCO_3$ 26, glucose 10 $CaCl_2$ 2, $MgCl_2$ 1, saturated with 95% O_2, 5% CO_2. At the University of Edinburgh, horizontal hippocampal slices (400 µm thick) were prepared in ice-cold ACSF containing NaCl, 86; NaH_2PO_4, 1.2; KCl, 25; $NaHCO_3$, 25; glucose, 20; sucrose, 75; $CaCl_2$, 0.5; $MgCl_2$, 7; saturated with 95% O_2, 5% CO_2 (Sigma-Aldrich). Slices were hemisected and an incision made through the CA1/CA3 boundary. Slices were initially recovered for 30 minutes at 32 ^oC then at room temperature for 2.5 hrs in ACSF containing (in mM): NaCl, 124; NaH_2PO_4, 1.2; KCl, 2.5; $NaHCO_3$, 25; glucose, 20; $CaCl_2$, 2; $MgCl_2$; 1, saturated with 95% O_2, 5% CO_2.

Electrophysiology

At MIT, field potential recordings were performed in a submersion chamber, perfused with ACSF (3–4 ml/min) at 30 °C. fEPSPs were recorded in CA1 stratum radiatum with extracellular electrodes filled with ACSF. Baseline responses were evoked by stimulation of the Schaffer collaterals at 0.033 Hz with a two-contact cluster electrode (FHC, Bowdoin, ME) using a 0.2 ms stimulus yielding 40–60% of the maximal response. Field recordings were filtered at 2 kHz, digitized at 50 kHz and analyzed using pClamp10 (Axon Instruments). Hippocampal slices were pre-incubated in ACSF containing either vehicle or GluN2 subtype specific blockers

conantokin-G (2 µM), Ro25-6981 (30 µM) and MPX-004 (30 µM) for 40 mins prior to recording, and then continually perfused throughout the entire experiment. NMDAR-dependent LTD and spine shrinkage was induced by the acute application of NMDA (20 µM, 3 min). The initial slope of the response was used to assess changes in synaptic strength. Functional LTD was quantified by comparing the average response 50–60 mins after NMDA, to the average of the last 10 mins of baseline. Isolated NMDA-mediated fEPSPs were obtained in ACSF containing Mg^{2+} (0.3 mM) glycine (1 µM), picrotoxin (100 µM) and NBQX (20 µM) before perfusing conantokin-G (2 µM), Ro25-6981 (30 µM) or MPX-004 (30 µM).

For extracellular recordings in CA3, an ACSF filled electrode was placed in the stratum pyramidal layer of CA3. Responses were recorded using PClamp10 software in voltage-clamp, amplified x1000, filtered between 300 Hz and 10 kHz and digitized at 25 kHz. A 10-minute baseline was recorded in ACSF before perfusing in either the $GABA_A$ antagonist bicuculline (50 µM) or the group 1 $mGluR_{1/5}$ agonist DHPG (50 µM). Voltage traces were Butterworth filtered between 300 and 1000 Hz before being downsampled by a factor of 10. The spike threshold was determined by calculating the median absolute deviation and multiplying by a factor of 5. Following spike detection, spikes were summed across 100 msec bins to reduce computational expense. To detect bursting events, a 500 msec sliding window was pulled across the entirety of the recording, from 5 to 60 minutes following the baseline period. A burst was identified if the spike rate within the window exceeded 8 Hz and was terminated in subsequent windows when the spike rate fell below 4 Hz.

At the University of Edinburgh, extracellular recordings in CA1 were performed by placing slices in a submersion chamber heated to 30 °C (Fine Science Tools) and perfused with pre-oxygenated ACSF at a rate of 4 ml/min. mGluR-dependent LTD was induced in CA1 by perfusing the slice with the group 1 mGluR agonist DHPG (50 µM, 5 mins). Waveform data was collected using WinLTP 1999-2009 (WinLTP Ltd., University of Bristol), amplified 1000 times (npi electronics), filtered at 1.3 kHz and digitized (National Instruments) at 20 kHz. The data was exported to Microsoft Excel and the magnitude of LTD was calculated from the last 10 minutes of the recording relative to the pre-drug baseline.

Two-photon laser-scanning microscopy

Time-lapse fluorescence two-photon imaging was performed using a Prairie Technologies Ultima system attached to an Olympus BX-51WI that was equipped with a mode-lock femtosecond-pulse Ti:Sapphire laser (Chameleon, Coherent). Experiments have been previously described in detail in [24]. Briefly, GFP was excited at 930 nm and images were taken with a 60X 0.9 NA objective lens, and a digital zoom of x 5.60 every 4 mins.

Metabolic Labeling

Hippocampi were rapidly dissected from mice and transverse hippocampal slices (500 µm) were prepared using a Stoelting tissue slicer in ice-cold artificial cerebrospinal fluid (ACSF) containing (in mM): NaCl, 124; NaH_2PO_4, 1.25; KCl, 3; $NaHCO_3$, 26; glucose, 10; $CaCl_2$, 2; $MgCl_2$, 1, saturated in 95% O_2 and 5% CO_2. Hippocampal slices were left to recover for at least 4 hours at 32°C in oxygenated ACSF. Transcription was blocked with actinomycin D (ActD, 25 µM; Tocris) ± drug for 30 minutes then slices were metabolically labelled in ^{35}S-Methionine/Cysteine express protein labeling mix (Perkin Elmer) ± drug for 30 minutes and snap frozen. Samples were homogenized in ice-cold buffer containing (in mM): HEPES, 10 pH 7.4; EDTA, 2; EGTA, 2; 1% triton X-100 (Sigma-Aldrich); protease and phosphatase inhibitors. Proteins were precipitated with TCA (Sigma-Aldrich) for 10 min on ice before being centrifuged at 16,000 rpm for 10 min and resolubilised in 1 M NaOH. The pH was adjusted with 0.33 M HCl and each sample was added to scintillation cocktail in triplicate and counts per minute (CPM) were quantified and normalised to overall protein using a DC protein assay kit II (Biorad). Inter-experimental variation in incorporation rates were corrected by normalising each value to the ^{35}S-Met/Cys ACSF and the average incorporation of all slices analyzed.

Image analysis

Throughout the baseline and LTD recording, a 512x512 pixel XY-scanned Z-series was taken every 4 minutes, at 1 µm of tissue depth for 15 µm of depth in total. Maximal fluorescence intensity of the Z-Series was summed to obtain a Z-stack for every time point and collated to form a movie montage, aligned using the StackReg function in Fiji/ImageJ (by Rasband, W.S., U. S. National Institutes of Health). Typically, 15 spines on multiple dendritic regions were tracked throughout the recording by outlining a 20 x 20 pixel region of interest (ROI). Within

this ROI, the total integrated fluorescence intensity of the green was calculated using ImageJ. Background fluorescence was tracked at 3 locations and subtracted, then overall fluorescence fluctuations was corrected by measuring the intensity over time at 4 locations. These values were then taken to be proportional to spine volume. As in our previous study [24], experiments showing <>7% of drift variation during the baseline period, calculated by fitting a linear regression line for the 30 min of baseline were excluded from analysis.

Audiogenic seizures

Male Fmr1 KO and WT mice (P17-25) were weighed and injected intraperitoneally (i.p.) with 1 mg/kg Glyx-13 or vehicle (saline) 1 hr prior to testing. Mice were habituated in the test chamber for 1 minute before they were exposed to a 120 dB audiogenic stimulation (recorded sampling of a modified personal alarm) for two minutes, which was monitored with a decibel meter. All genotype and treatment conditions were tested within a session, with the experimenter blind to genotype and treatment. Incidence of seizures was scored based on whether the mice exhibited wild running, clonic seizure or tonic seizure.

Quantification and statistical analysis

All data is expressed as a mean ± S.E.M with N representing the number of animals. Statistical analyses were performed using GraphPad Prism 9.0 with a confidence level set at 95%. Outliers (±2 SD from the mean) were removed and significant effects determined using Student's *t*-test or one-way ANOVA with Bonferroni *post-hoc* test (single comparisons) or repeated-measures 2-way ANOVA followed by paired Student's *t*-test (multiple comparisons). AGS incidence scores were analyzed using Fisher's Exact test.

Cited Literature

1. Liu, S., Zhou, L., Yuan, H., Vieira, M., Sanz-Clemente, A., Badger, J.D., 2nd, Lu, W., Traynelis, S.F., and Roche, K.W. (2017). A Rare Variant Identified Within the GluN2B C-Terminus in a Patient with Autism Affects NMDA Receptor Surface Expression and Spine Density. J Neurosci *37*, 4093-4102. 10.1523/JNEUROSCI.0827-16.2017.
2. O'Roak, B.J., Vives, L., Fu, W., Egertson, J.D., Stanaway, I.B., Phelps, I.G., Carvill, G., Kumar, A., Lee, C., Ankenman, K., et al. (2012). Multiplex targeted sequencing identifies recurrently mutated genes in autism spectrum disorders. Science *338*, 1619-1622. 10.1126/science.1227764.
3. Xu, X.X., and Luo, J.H. (2018). Mutations of N-Methyl-D-Aspartate Receptor Subunits in Epilepsy. Neurosci Bull *34*, 549-565. 10.1007/s12264-017-0191-5.
4. Lee, H.K., Kameyama, K., Huganir, R.L., and Bear, M.F. (1998). NMDA induces long-term synaptic depression and dephosphorylation of the GluR1 subunit of AMPA receptors in hippocampus. Neuron *21*, 1151-1162.
5. Halpain, S., Hipolito, A., and Saffer, L. (1998). Regulation of F-actin stability in dendritic spines by glutamate receptors and calcineurin. J Neurosci *18*, 9835-9844. 10.1523/JNEUROSCI.18-23-09835.1998.
6. Beattie, E.C., Carroll, R.C., Yu, X., Morishita, W., Yasuda, H., von Zastrow, M., and Malenka, R.C. (2000). Regulation of AMPA receptor endocytosis by a signaling mechanism shared with LTD. Nat Neurosci *3*, 1291-1300. 10.1038/81823.
7. Dudek, S.M., and Bear, M.F. (1992). Homosynaptic long-term depression in area CA1 of hippocampus and effects of N-methyl-D-aspartate receptor blockade. Proceedings of the National Academy of Sciences of the United States of America *89*, 4363-4367. 10.1073/pnas.89.10.4363.
8. Zhou, Q., Homma, K.J., and Poo, M.M. (2004). Shrinkage of dendritic spines associated with long-term depression of hippocampal synapses. Neuron *44*, 749-757. 10.1016/j.neuron.2004.11.011.
9. Mulkey, R.M., and Malenka, R.C. (1992). Mechanisms underlying induction of homosynaptic long-term depression in area CA1 of the hippocampus. Neuron *9*, 967-975. 10.1016/0896-6273(92)90248-c.

10. Stein, I.S., Gray, J.A., and Zito, K. (2015). Non-Ionotropic NMDA Receptor Signaling Drives Activity-Induced Dendritic Spine Shrinkage. J Neurosci *35*, 12303-12308. 10.1523/JNEUROSCI.4289-14.2015.
11. Dore, K., Aow, J., and Malinow, R. (2015). Agonist binding to the NMDA receptor drives movement of its cytoplasmic domain without ion flow. Proceedings of the National Academy of Sciences of the United States of America *112*, 14705-14710. 10.1073/pnas.1520023112.
12. Stein, I.S., Park, D.K., Flores, J.C., Jahncke, J.N., and Zito, K. (2020). Molecular Mechanisms of Non-ionotropic NMDA Receptor Signaling in Dendritic Spine Shrinkage. J Neurosci *40*, 3741-3750. 10.1523/JNEUROSCI.0046-20.2020.
13. Stein, I.S., Park, D.K., Claiborne, N., and Zito, K. (2021). Non-ionotropic NMDA receptor signaling gates bidirectional structural plasticity of dendritic spines. Cell Rep *34*, 108664. 10.1016/j.celrep.2020.108664.
14. Nabavi, S., Kessels, H.W., Alfonso, S., Aow, J., Fox, R., and Malinow, R. (2013). Metabotropic NMDA receptor function is required for NMDA receptor-dependent long-term depression. Proceedings of the National Academy of Sciences of the United States of America *110*, 4027-4032. 10.1073/pnas.1219454110.
15. Babiec, W.E., Guglietta, R., Jami, S.A., Morishita, W., Malenka, R.C., and O'Dell, T.J. (2014). Ionotropic NMDA receptor signaling is required for the induction of long-term depression in the mouse hippocampal CA1 region. J Neurosci *34*, 5285-5290. 10.1523/JNEUROSCI.5419-13.2014.
16. Coultrap, S.J., Freund, R.K., O'Leary, H., Sanderson, J.L., Roche, K.W., Dell'Acqua, M.L., and Bayer, K.U. (2014). Autonomous CaMKII mediates both LTP and LTD using a mechanism for differential substrate site selection. Cell Rep *6*, 431-437. 10.1016/j.celrep.2014.01.005.
17. Sanderson, J.L., Gorski, J.A., and Dell'Acqua, M.L. (2016). NMDA Receptor-Dependent LTD Requires Transient Synaptic Incorporation of Ca(2)(+)-Permeable AMPARs Mediated by AKAP150-Anchored PKA and Calcineurin. Neuron *89*, 1000-1015. 10.1016/j.neuron.2016.01.043.
18. Dupuis, J.P., Nicole, O., and Groc, L. (2023). NMDA receptor functions in health and disease: Old actor, new dimensions. Neuron *111*, 2312-2328. 10.1016/j.neuron.2023.05.002.
19. Dunot, J., Moreno, S., Gandin, C., Pousinha, P.A., Amici, M., Dupuis, J., Anisimova, M., Winschel, A., Uriot, M., Petshow, S.J., et al. (2024). APP fragment controls both

ionotropic and non-ionotropic signaling of NMDA receptors. Neuron. 10.1016/j.neuron.2024.05.027.

20. Carter, B.C., and Jahr, C.E. (2016). Postsynaptic, not presynaptic NMDA receptors are required for spike-timing-dependent LTD induction. Nat Neurosci *19*, 1218-1224. 10.1038/nn.4343.
21. Wong, J.M., and Gray, J.A. (2018). Long-Term Depression Is Independent of GluN2 Subunit Composition. J Neurosci *38*, 4462-4470. 10.1523/JNEUROSCI.0394-18.2018.
22. Dore, K., and Malinow, R. (2021). Elevated PSD-95 Blocks Ion-flux Independent LTD: A Potential New Role for PSD-95 in Synaptic Plasticity. Neuroscience *456*, 43-49. 10.1016/j.neuroscience.2020.02.020.
23. Barragan, E.V., Anisimova, M., Vijayakumar, V., Coblentz, A., Park, D.K., Salaka, R.J., Nisan, A.F.K., Petshow, S., Dore, K., Zito, K., and Gray, J.A. (2024). d-Serine Inhibits Non-ionotropic NMDA Receptor Signaling. J Neurosci *44*. 10.1523/JNEUROSCI.0140-24.2024.
24. Thomazeau, A., Bosch, M., Essayan-Perez, S., Barnes, S.A., De Jesus-Cortes, H., and Bear, M.F. (2021). Dissociation of functional and structural plasticity of dendritic spines during NMDAR and mGluR-dependent long-term synaptic depression in wild-type and fragile X model mice. Molecular psychiatry *26*, 4652-4669. 10.1038/s41380-020-0821-6.
25. Kessels, H.W., Nabavi, S., and Malinow, R. (2013). Metabotropic NMDA receptor function is required for beta-amyloid-induced synaptic depression. Proceedings of the National Academy of Sciences of the United States of America *110*, 4033-4038. 10.1073/pnas.1219605110.
26. Grossman, A.W., Elisseou, N.M., McKinney, B.C., and Greenough, W.T. (2006). Hippocampal pyramidal cells in adult Fmr1 knockout mice exhibit an immature-appearing profile of dendritic spines. Brain Res *1084*, 158-164. 10.1016/j.brainres.2006.02.044.
27. Huber, K.M., Gallagher, S.M., Warren, S.T., and Bear, M.F. (2002). Altered synaptic plasticity in a mouse model of fragile X mental retardation. Proceedings of the National Academy of Sciences of the United States of America *99*, 7746-7750. 10.1073/pnas.122205699.
28. Osterweil, E.K., Krueger, D.D., Reinhold, K., and Bear, M.F. (2010). Hypersensitivity to mGluR5 and ERK1/2 leads to excessive protein synthesis in the

hippocampus of a mouse model of fragile X syndrome. J Neurosci *30*, 15616-15627. 10.1523/JNEUROSCI.3888-10.2010.

29. Sun, W., Hansen, K.B., and Jahr, C.E. (2017). Allosteric Interactions between NMDA Receptor Subunits Shape the Developmental Shift in Channel Properties. Neuron *94*, 58-64 e53. 10.1016/j.neuron.2017.03.018.
30. Philpot, B.D., and Zukin, R.S. (2010). Synapse-specific metaplasticity: to be silenced is not to silence 2B. Neuron *66*, 814-816. 10.1016/j.neuron.2010.06.014.
31. Li, Y., Erzurumlu, R.S., Chen, C., Jhaveri, S., and Tonegawa, S. (1994). Whisker-related neuronal patterns fail to develop in the trigeminal brainstem nuclei of NMDAR1 knockout mice. Cell *76*, 427-437. 10.1016/0092-8674(94)90108-2.
32. Iwasato, T., Datwani, A., Wolf, A.M., Nishiyama, H., Taguchi, Y., Tonegawa, S., Knopfel, T., Erzurumlu, R.S., and Itohara, S. (2000). Cortex-restricted disruption of NMDAR1 impairs neuronal patterns in the barrel cortex. Nature *406*, 726-731. 10.1038/35021059.
33. Gray, J.A., Shi, Y., Usui, H., During, M.J., Sakimura, K., and Nicoll, R.A. (2011). Distinct modes of AMPA receptor suppression at developing synapses by GluN2A and GluN2B: single-cell NMDA receptor subunit deletion in vivo. Neuron *71*, 1085-1101. 10.1016/j.neuron.2011.08.007.
34. Paoletti, P., Bellone, C., and Zhou, Q. (2013). NMDA receptor subunit diversity: impact on receptor properties, synaptic plasticity and disease. Nature reviews. Neuroscience *14*, 383-400. 10.1038/nrn3504.
35. Ryan, T.J., Emes, R.D., Grant, S.G., and Komiyama, N.H. (2008). Evolution of NMDA receptor cytoplasmic interaction domains: implications for organisation of synaptic signalling complexes. BMC neuroscience *9*, 6. 10.1186/1471-2202-9-6.
36. Volkmann, R.A., Fanger, C.M., Anderson, D.R., Sirivolu, V.R., Paschetto, K., Gordon, E., Virginio, C., Gleyzes, M., Buisson, B., Steidl, E., et al. (2016). MPX-004 and MPX-007: New Pharmacological Tools to Study the Physiology of NMDA Receptors Containing the GluN2A Subunit. PloS one *11*, e0148129. 10.1371/journal.pone.0148129.
37. Donevan, S.D., and McCabe, R.T. (2000). Conantokin G is an NR2B-selective competitive antagonist of N-methyl-D-aspartate receptors. Mol Pharmacol *58*, 614-623. 10.1124/mol.58.3.614.
38. Yi, F., Mou, T.C., Dorsett, K.N., Volkmann, R.A., Menniti, F.S., Sprang, S.R., and Hansen, K.B. (2016). Structural Basis for Negative Allosteric Modulation of

GluN2A-Containing NMDA Receptors. Neuron *91*, 1316-1329. 10.1016/j.neuron.2016.08.014.

39. Stroebel, D., Casado, M., and Paoletti, P. (2018). Triheteromeric NMDA receptors: from structure to synaptic physiology. Curr Opin Physiol *2*, 1-12. 10.1016/j.cophys.2017.12.004.
40. Ryan, T.J., Kopanitsa, M.V., Indersmitten, T., Nithianantharajah, J., Afinowi, N.O., Pettit, C., Stanford, L.E., Sprengel, R., Saksida, L.M., Bussey, T.J., et al. (2013). Evolution of GluN2A/B cytoplasmic domains diversified vertebrate synaptic plasticity and behavior. Nat Neurosci *16*, 25-32. 10.1038/nn.3277.
41. Tang, G., Gudsnuk, K., Kuo, S.H., Cotrina, M.L., Rosoklija, G., Sosunov, A., Sonders, M.S., Kanter, E., Castagna, C., Yamamoto, A., et al. (2014). Loss of mTOR-dependent macroautophagy causes autistic-like synaptic pruning deficits. Neuron *83*, 1131-1143. 10.1016/j.neuron.2014.07.040.
42. Auerbach, B.D., Osterweil, E.K., and Bear, M.F. (2011). Mutations causing syndromic autism define an axis of synaptic pathophysiology. Nature *480*, 63-68. 10.1038/nature10658.
43. Thomson, S.R., Seo, S.S., Barnes, S.A., Louros, S.R., Muscas, M., Dando, O., Kirby, C., Wyllie, D.J.A., Hardingham, G.E., Kind, P.C., and Osterweil, E.K. (2017). Cell-Type-Specific Translation Profiling Reveals a Novel Strategy for Treating Fragile X Syndrome. Neuron *95*, 550-563 e555. 10.1016/j.neuron.2017.07.013.
44. Huber, K.M., Kayser, M.S., and Bear, M.F. (2000). Role for rapid dendritic protein synthesis in hippocampal mGluR-dependent long-term depression. Science *288*, 1254-1257.
45. Nosyreva, E.D., and Huber, K.M. (2006). Metabotropic receptor-dependent long-term depression persists in the absence of protein synthesis in the mouse model of fragile X syndrome. Journal of neurophysiology *95*, 3291-3295. 10.1152/jn.01316.2005.
46. Barnes, S.A., Wijetunge, L.S., Jackson, A.D., Katsanevaki, D., Osterweil, E.K., Komiyama, N.H., Grant, S.G., Bear, M.F., Nagerl, U.V., Kind, P.C., and Wyllie, D.J. (2015). Convergence of hippocampal pathophysiology in Syngap+/- and Fmr1-/y mice. J Neurosci *35*, 15073-15081. 10.1523/JNEUROSCI.1087-15.2015.
47. Huber, K.M., Roder, J.C., and Bear, M.F. (2001). Chemical induction of mGluR5- and protein synthesis--dependent long-term depression in hippocampal area CA1. Journal of neurophysiology *86*, 321-325. 10.1152/jn.2001.86.1.321.

48. Michalon, A., Sidorov, M., Ballard, T.M., Ozmen, L., Spooren, W., Wettstein, J.G., Jaeschke, G., Bear, M.F., and Lindemann, L. (2012). Chronic pharmacological mGlu5 inhibition corrects fragile X in adult mice. Neuron *74*, 49-56. 10.1016/j.neuron.2012.03.009.

49. Merlin, L.R., Bergold, P.J., and Wong, R.K. (1998). Requirement of protein synthesis for group I mGluR-mediated induction of epileptiform discharges. Journal of neurophysiology *80*, 989-993. 10.1152/jn.1998.80.2.989.

50. Osterweil, E.K., Chuang, S.C., Chubykin, A.A., Sidorov, M., Bianchi, R., Wong, R.K., and Bear, M.F. (2013). Lovastatin corrects excess protein synthesis and prevents epileptogenesis in a mouse model of fragile X syndrome. Neuron *77*, 243-250. 10.1016/j.neuron.2012.01.034.

51. Dolen, G., Osterweil, E., Rao, B.S., Smith, G.B., Auerbach, B.D., Chattarji, S., and Bear, M.F. (2007). Correction of fragile X syndrome in mice. Neuron *56*, 955-962. 10.1016/j.neuron.2007.12.001.

52. Donello, J.E., Banerjee, P., Li, Y.X., Guo, Y.X., Yoshitake, T., Zhang, X.L., Miry, O., Kehr, J., Stanton, P.K., Gross, A.L., et al. (2019). Positive N-Methyl-D-Aspartate Receptor Modulation by Rapastinel Promotes Rapid and Sustained Antidepressant-Like Effects. Int J Neuropsychopharmacol *22*, 247-259. 10.1093/ijnp/pyy101.

53. Zhang, X.L., Sullivan, J.A., Moskal, J.R., and Stanton, P.K. (2008). A NMDA receptor glycine site partial agonist, GLYX-13, simultaneously enhances LTP and reduces LTD at Schaffer collateral-CA1 synapses in hippocampus. Neuropharmacology *55*, 1238-1250. 10.1016/j.neuropharm.2008.08.018.

54. Moskal, J.R., Burch, R., Burgdorf, J.S., Kroes, R.A., Stanton, P.K., Disterhoft, J.F., and Leander, J.D. (2014). GLYX-13, an NMDA receptor glycine site functional partial agonist enhances cognition and produces antidepressant effects without the psychotomimetic side effects of NMDA receptor antagonists. Expert Opin Investig Drugs *23*, 243-254. 10.1517/13543784.2014.852536.

55. Moskal, J.R., Burgdorf, J., Kroes, R.A., Brudzynski, S.M., and Panksepp, J. (2011). A novel NMDA receptor glycine-site partial agonist, GLYX-13, has therapeutic potential for the treatment of autism. Neuroscience and biobehavioral reviews *35*, 1982-1988. 10.1016/j.neubiorev.2011.06.006.

56. Burgdorf, J., Zhang, X.L., Weiss, C., Matthews, E., Disterhoft, J.F., Stanton, P.K., and Moskal, J.R. (2011). The N-methyl-D-aspartate receptor modulator GLYX-13

enhances learning and memory, in young adult and learning impaired aging rats. Neurobiol Aging *32*, 698-706. 10.1016/j.neurobiolaging.2009.04.012.

57. Frank, R.A., Komiyama, N.H., Ryan, T.J., Zhu, F., O'Dell, T.J., and Grant, S.G. (2016). NMDA receptors are selectively partitioned into complexes and supercomplexes during synapse maturation. Nat Commun *7*, 11264. 10.1038/ncomms11264.
58. Vissel, B., Krupp, J.J., Heinemann, S.F., and Westbrook, G.L. (2001). A use-dependent tyrosine dephosphorylation of NMDA receptors is independent of ion flux. Nat Neurosci *4*, 587-596. 10.1038/88404.
59. Hu, R., Chen, J., Lujan, B., Lei, R., Zhang, M., Wang, Z., Liao, M., Li, Z., Wan, Y., Liu, F., et al. (2016). Glycine triggers a non-ionotropic activity of GluN2A-containing NMDA receptors to confer neuroprotection. Sci Rep *6*, 34459. 10.1038/srep34459.
60. Rajani, V., Sengar, A.S., and Salter, M.W. (2020). Tripartite signalling by NMDA receptors. Mol Brain *13*, 23. 10.1186/s13041-020-0563-z.
61. Nosyreva, E.D., and Huber, K.M. (2005). Developmental switch in synaptic mechanisms of hippocampal metabotropic glutamate receptor-dependent long-term depression. J Neurosci *25*, 2992-3001. 25/11/2992 [pii]

10.1523/JNEUROSCI.3652-04.2005.

62. Chen, W.S., and Bear, M.F. (2007). Activity-dependent regulation of NR2B translation contributes to metaplasticity in mouse visual cortex. Neuropharmacology *52*, 200-214. 10.1016/j.neuropharm.2006.07.003.
63. Miller, O.H., Yang, L., Wang, C.C., Hargroder, E.A., Zhang, Y., Delpire, E., and Hall, B.J. (2014). GluN2B-containing NMDA receptors regulate depression-like behavior and are critical for the rapid antidepressant actions of ketamine. Elife *3*, e03581. 10.7554/eLife.03581.
64. Wang, C.C., Held, R.G., and Hall, B.J. (2013). SynGAP regulates protein synthesis and homeostatic synaptic plasticity in developing cortical networks. PloS one *8*, e83941. 10.1371/journal.pone.0083941.
65. Hien, A., Molinaro, G., Liu, B., Huber, K.M., and Richter, J.D. (2020). Ribosome profiling in mouse hippocampus: plasticity-induced regulation and bidirectional control by TSC2 and FMRP. Molecular autism *11*, 78. 10.1186/s13229-020-00384-9.
66. Seo, S.S., Louros, S.R., Anstey, N., Gonzalez-Lozano, M.A., Harper, C.B., Verity, N.C., Dando, O., Thomson, S.R., Darnell, J.C., Kind, P.C., et al. (2022). Excess

ribosomal protein production unbalances translation in a model of Fragile X Syndrome. Nat Commun *13*, 3236. 10.1038/s41467-022-30979-0.

67. Auerbach, B.D., and Bear, M.F. (2010). Loss of the fragile X mental retardation protein decouples metabotropic glutamate receptor dependent priming of long-term potentiation from protein synthesis. Journal of neurophysiology *104*, 1047-1051. 10.1152/jn.00449.2010.

68. Chuang, S.C., Zhao, W., Bauchwitz, R., Yan, Q., Bianchi, R., and Wong, R.K. (2005). Prolonged epileptiform discharges induced by altered group I metabotropic glutamate receptor-mediated synaptic responses in hippocampal slices of a fragile X mouse model. J Neurosci *25*, 8048-8055. 25/35/8048 [pii] 10.1523/JNEUROSCI.1777-05.2005.

69. Bateup, H.S., Takasaki, K.T., Saulnier, J.L., Denefrio, C.L., and Sabatini, B.L. (2011). Loss of Tsc1 in vivo impairs hippocampal mGluR-LTD and increases excitatory synaptic function. J Neurosci *31*, 8862-8869. 10.1523/JNEUROSCI.1617-11.2011.

70. Tao, J., Wu, H., Coronado, A.A., de Laittre, E., Osterweil, E.K., Zhang, Y., and Bear, M.F. (2016). Negative Allosteric Modulation of mGluR5 Partially Corrects Pathophysiology in a Mouse Model of Rett Syndrome. J Neurosci *36*, 11946-11958. 10.1523/JNEUROSCI.0672-16.2016.

71. Tian, D., Stoppel, L.J., Heynen, A.J., Lindemann, L., Jaeschke, G., Mills, A.A., and Bear, M.F. (2015). Contribution of mGluR5 to pathophysiology in a mouse model of human chromosome 16p11.2 microdeletion. Nat Neurosci *18*, 182-184. 10.1038/nn.3911.

72. Silverman, J.L., Smith, D.G., Rizzo, S.J., Karras, M.N., Turner, S.M., Tolu, S.S., Bryce, D.K., Smith, D.L., Fonseca, K., Ring, R.H., and Crawley, J.N. (2012). Negative allosteric modulation of the mGluR5 receptor reduces repetitive behaviors and rescues social deficits in mouse models of autism. Sci Transl Med *4*, 131ra151. 10.1126/scitranslmed.3003501.

73. Stoppel, L.J., Osterweil, E.K., and Bear, M.F. (2017). The mGluR Theory of Fragile X: From Mice to Men. In Fragile X Syndrome, R. Wilemsen, and R.F. Kooy, eds. (Academic Press), pp. 173-204. 10.1016/B978-0-12-804461-2.00009-3.

74. Greenblatt, E.J., and Spradling, A.C. (2018). Fragile X mental retardation 1 gene enhances the translation of large autism-related proteins. Science *361*, 709-712. 10.1126/science.aas9963.

75. Louros, S.R., Seo, S.S., Maio, B., Martinez-Gonzalez, C., Gonzalez-Lozano, M.A., Muscas, M., Verity, N.C., Wills, J.C., Li, K.W., Nolan, M.F., and Osterweil, E.K. (2023). Excessive proteostasis contributes to pathology in fragile X syndrome. Neuron *111*, 508-525 e507. 10.1016/j.neuron.2022.11.012.

76. Moskal, J.R., Kuo, A.G., Weiss, C., Wood, P.L., O'Connor Hanson, A., Kelso, S., Harris, R.B., and Disterhoft, J.F. (2005). GLYX-13: a monoclonal antibody-derived peptide that acts as an N-methyl-D-aspartate receptor modulator. Neuropharmacology *49*, 1077-1087. 10.1016/j.neuropharm.2005.06.006.

77. McCamphill, P.K., Stoppel, L.J., Senter, R.K., Lewis, M.C., Heynen, A.J., Stoppel, D.C., Sridhar, V., Collins, K.A., Shi, X., Pan, J.Q., et al. (2020). Selective inhibition of glycogen synthase kinase 3alpha corrects pathophysiology in a mouse model of fragile X syndrome. Sci Transl Med *12*. 10.1126/scitranslmed.aam8572.

78. Moskal, J.R., Burgdorf, J.S., Stanton, P.K., Kroes, R.A., Disterhoft, J.F., Burch, R.M., and Khan, M.A. (2017). The Development of Rapastinel (Formerly GLYX-13); A Rapid Acting and Long Lasting Antidepressant. Curr Neuropharmacol *15*, 47-56. 10.2174/1570159x14666160321122703.

79. Lemke, J.R., Hendrickx, R., Geider, K., Laube, B., Schwake, M., Harvey, R.J., James, V.M., Pepler, A., Steiner, I., Hortnagel, K., et al. (2014). GRIN2B mutations in West syndrome and intellectual disability with focal epilepsy. Ann Neurol *75*, 147-154. 10.1002/ana.24073.

80. Zhang, Y., Kong, W., Gao, Y., Liu, X., Gao, K., Xie, H., Wu, Y., Zhang, Y., Wang, J., Gao, F., et al. (2015). Gene Mutation Analysis in 253 Chinese Children with Unexplained Epilepsy and Intellectual/Developmental Disabilities. PloS one *10*, e0141782. 10.1371/journal.pone.0141782.

81. Epi, K.C., Epilepsy Phenome/Genome, P., Allen, A.S., Berkovic, S.F., Cossette, P., Delanty, N., Dlugos, D., Eichler, E.E., Epstein, M.P., Glauser, T., et al. (2013). De novo mutations in epileptic encephalopathies. Nature *501*, 217-221. 10.1038/nature12439.

82. Monyer, H., Burnashev, N., Laurie, D.J., Sakmann, B., and Seeburg, P.H. (1994). Developmental and regional expression in the rat brain and functional properties of four NMDA receptors. Neuron *12*, 529-540. 10.1016/0896-6273(94)90210-0.

83. Cossenza, M., Cadilhe, D.V., Coutinho, R.N., and Paes-de-Carvalho, R. (2006). Inhibition of protein synthesis by activation of NMDA receptors in cultured retinal

cells: a new mechanism for the regulation of nitric oxide production. J Neurochem *97*, 1481-1493. 10.1111/j.1471-4159.2006.03843.x.

84. Sutton, M.A., Ito, H.T., Cressy, P., Kempf, C., Woo, J.C., and Schuman, E.M. (2006). Miniature neurotransmission stabilizes synaptic function via tonic suppression of local dendritic protein synthesis. Cell *125*, 785-799. 10.1016/j.cell.2006.03.040.
85. Lee, H.K., Barbarosie, M., Kameyama, K., Bear, M.F., and Huganir, R.L. (2000). Regulation of distinct AMPA receptor phosphorylation sites during bidirectional synaptic plasticity. Nature *405*, 955-959. 10.1038/35016089.
86. Oh, W.C., Hill, T.C., and Zito, K. (2013). Synapse-specific and size-dependent mechanisms of spine structural plasticity accompanying synaptic weakening. Proceedings of the National Academy of Sciences of the United States of America *110*, E305-312. 10.1073/pnas.1214705110.
87. Jang, J., Anisimova, M., Oh, W.C., and Zito, K. (2021). Induction of input-specific spine shrinkage on dendrites of rodent hippocampal CA1 neurons using two-photon glutamate uncaging. STAR Protoc *2*, 100996. 10.1016/j.xpro.2021.100996.
88. Barton, M.E., White, H.S., and Wilcox, K.S. (2004). The effect of CGX-1007 and CI-1041, novel NMDA receptor antagonists, on NMDA receptor-mediated EPSCs. Epilepsy Res *59*, 13-24. 10.1016/j.eplepsyres.2003.12.011.
89. Tovar, K.R., McGinley, M.J., and Westbrook, G.L. (2013). Triheteromeric NMDA receptors at hippocampal synapses. J Neurosci *33*, 9150-9160. 10.1523/JNEUROSCI.0829-13.2013.
90. Feng, G., Mellor, R.H., Bernstein, M., Keller-Peck, C., Nguyen, Q.T., Wallace, M., Nerbonne, J.M., Lichtman, J.W., and Sanes, J.R. (2000). Imaging neuronal subsets in transgenic mice expressing multiple spectral variants of GFP. Neuron *28*, 41-51. 10.1016/s0896-6273(00)00084-2.
91. Townsend, M., Yoshii, A., Mishina, M., and Constantine-Paton, M. (2003). Developmental loss of miniature N-methyl-D-aspartate receptor currents in NR2A knockout mice. Proceedings of the National Academy of Sciences of the United States of America *100*, 1340-1345. 10.1073/pnas.0335786100.

Figure 1

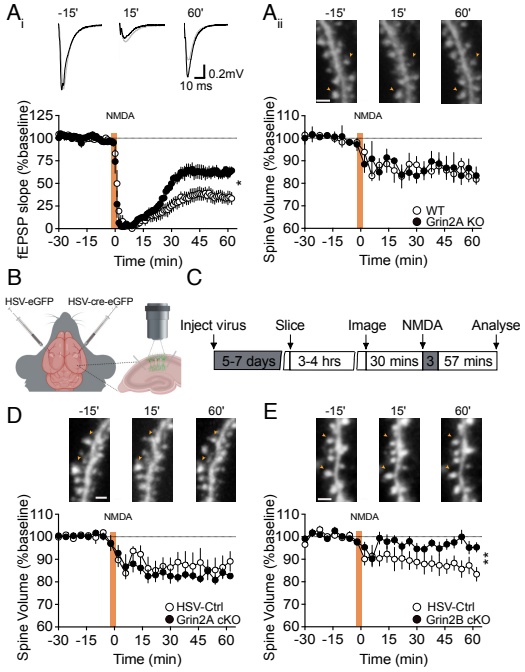
A
i
-15'
15'
60'
0.2mV
10 ms
NMDA
fEPSP slope (%baseline)
Time (min)
A
ii
-15'
15'
60'
NMDA
Spine Volume (%baseline)
WT
Grin2A KO
Time (min)
B
HSV-eGFP
HSV-cre-eGFP
C
Inject virus
Slice
Image
NMDA
Analyse
5-7 days
3-4 hrs
30 mins
3
57 mins
D
-15'
15'
60'
NMDA
Spine Volume (%baseline)
HSV-Ctrl
Grin2A cKO
Time (min)
E
-15'
15'
60'
NMDA
Spine Volume (%baseline)
HSV-Ctrl
Grin2B cKO
Time (min)

Figure 2

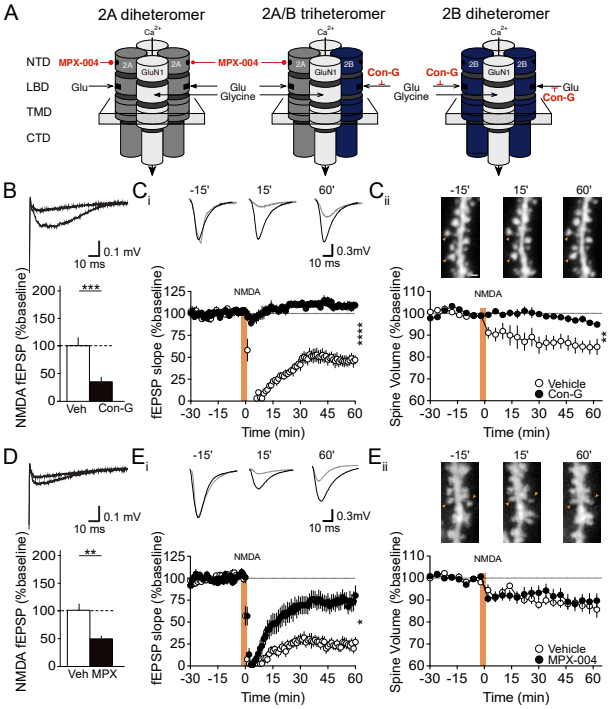
A
2A diheteromer
2A/B triheteromer
2B diheteromer
NTD
LBD
TMD
CTD
MPX-004
Glu
Glu
Glycine
Con-G
B
C
D
E
0.1 mV
10 ms
0.3mV
-15'
15'
60'
NMDA fEPSP (%baseline)
fEPSP slope (%baseline)
Spine Volume (%baseline)
Time (min)
NMDA
Veh
Con-G
MPX
Vehicle
MPX-004

Figure 3

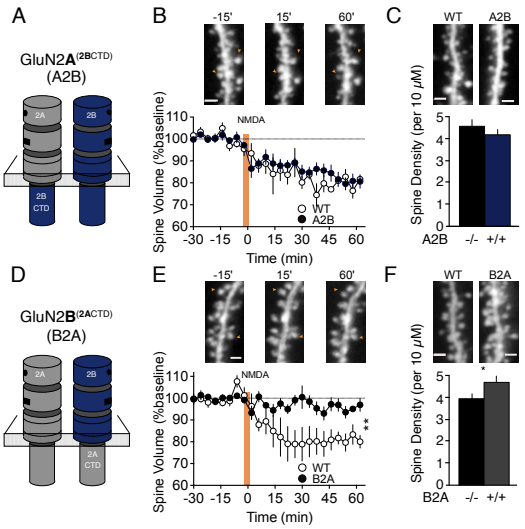
A
GluN2A(2BCTD)
(A2B)
2A
2B
2B CTD
B
-15'
15'
60'
NMDA
Spine Volume (%baseline)
110
100
90
80
70
60
-30 -15 0 15 30 45 60
Time (min)
WT
A2B
C
WT
A2B
Spine Density (per 10 μM)
5
4
3
2
1
0
A2B -/- +/+
D
GluN2B(2ACTD)
(B2A)
2A
2B
2A CTD
E
-15'
15'
60'
NMDA
Spine Volume (%baseline)
110
100
90
80
70
60
-30 -15 0 15 30 45 60
Time (min)
WT
B2A
F
WT
B2A
Spine Density (per 10 μM)
5
4
3
2
1
0
B2A -/- +/+

Figure 4

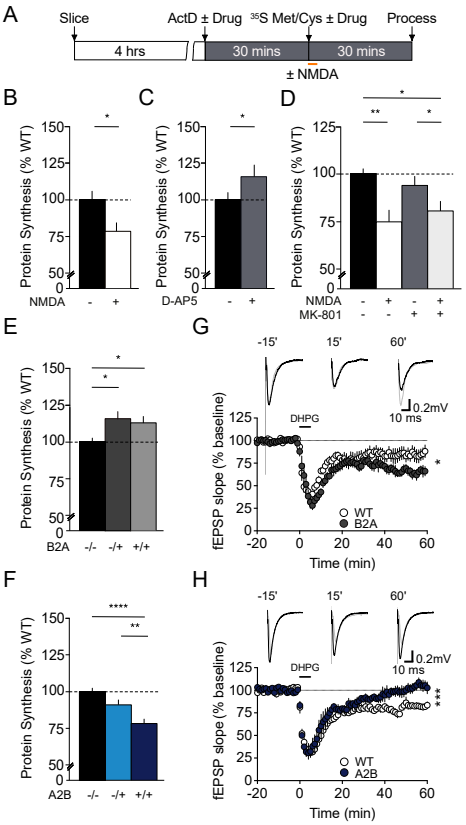
A
Slice
ActD ± Drug
35S Met/Cys ± Drug
Process
4 hrs
30 mins
30 mins
± NMDA
B
C
D
Protein Synthesis (% WT)
NMDA
D-AP5
MK-801
E
F
B2A
A2B
-/-
-/+
+/+
G
H
-15'
15'
60'
DHPG
0.2mV
10 ms
fEPSP slope (% baseline)
Time (min)
WT
B2A
A2B

Figure 5

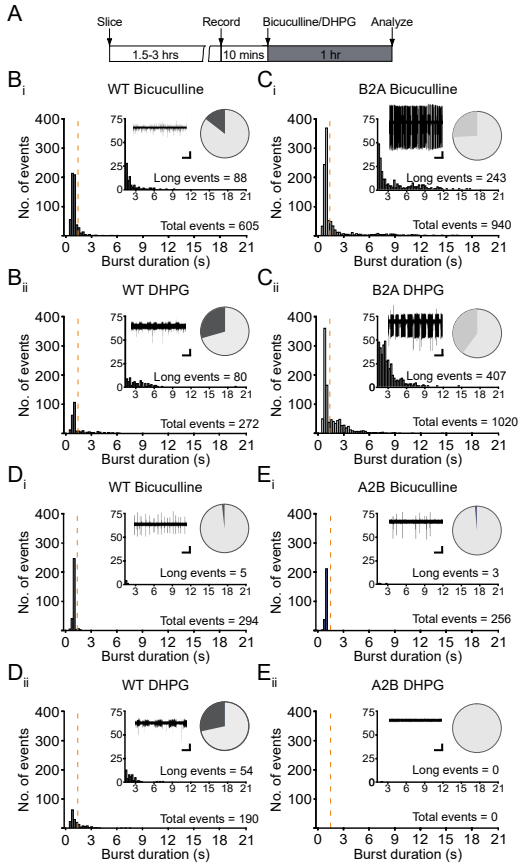
A
Slice
Record
Bicuculline/DHPG
Analyze
1.5-3 hrs
10 mins
1 hr
B_i
WT Bicuculline
Long events = 88
Total events = 605
C_i
B2A Bicuculline
Long events = 243
Total events = 940
B_ii
WT DHPG
Long events = 80
Total events = 272
C_ii
B2A DHPG
Long events = 407
Total events = 1020
D_i
WT Bicuculline
Long events = 5
Total events = 294
E_i
A2B Bicuculline
Long events = 3
Total events = 256
D_ii
WT DHPG
Long events = 54
Total events = 190
E_ii
A2B DHPG
Long events = 0
Total events = 0
No. of events
Burst duration (s)

Figure 6

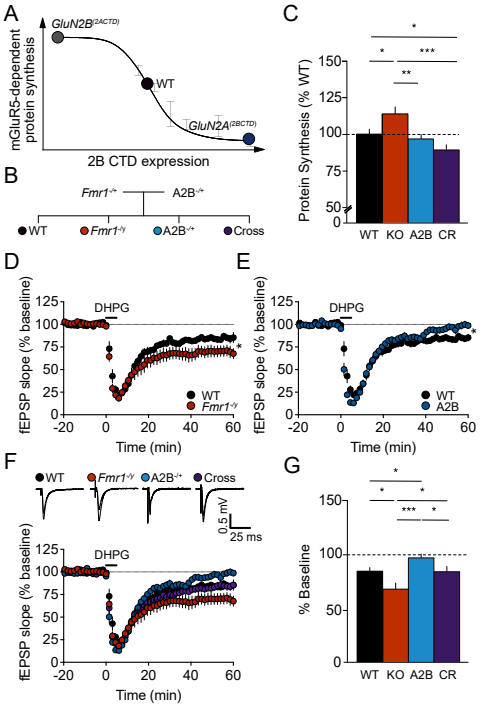
A
GluN2B(2ACTD)
mGluR5-dependent protein synthesis
WT
GluN2A(2BCTD)
2B CTD expression
B
Fmr1-/+
A2B-/+
WT
Fmr1-/y
A2B-/+
Cross
C
Protein Synthesis (% WT)
150
125
100
75
50
0
WT KO A2B CR
D
fEPSP slope (% baseline)
DHPG
WT
Fmr1-/y
Time (min)
E
fEPSP slope (% baseline)
DHPG
WT
A2B
Time (min)
F
WT
Fmr1-/y
A2B-/+
Cross
0.5 mV
25 ms
fEPSP slope (% baseline)
DHPG
Time (min)
G
% Baseline
WT KO A2B CR

Figure 7

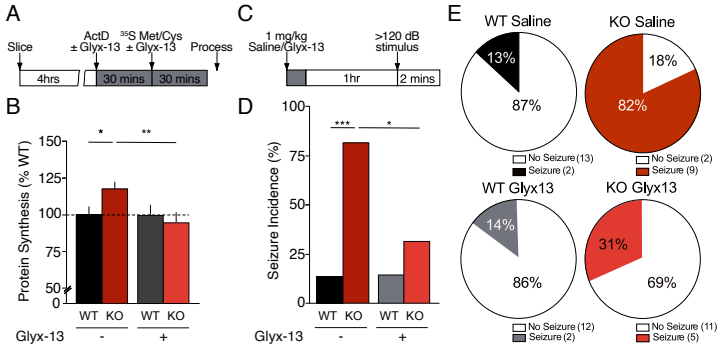
A
Slice
ActD ± Glyx-13
35S Met/Cys ± Glyx-13
Process
4hrs
30 mins
30 mins
B
Protein Synthesis (% WT)
150
125
100
75
50
0
*
**
WT KO WT KO
Glyx-13 - +
C
1 mg/kg Saline/Glyx-13
>120 dB stimulus
1hr
2 mins
D
Seizure Incidence (%)
100
75
50
25
0
***
*
WT KO WT KO
Glyx-13 - +
E
WT Saline
13%
87%
No Seizure (13)
Seizure (2)
KO Saline
18%
82%
No Seizure (2)
Seizure (9)
WT Glyx13
14%
86%
No Seizure (12)
Seizure (2)
KO Glyx13
31%
69%
No Seizure (11)
Seizure (5)
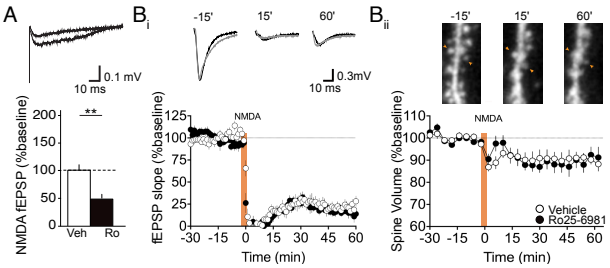
Supplementary Figure 1